



Influence of the wintertime North Atlantic Oscillation on European tropospheric composition: an observational and modelling study

Richard J. Pope^{1,2}, Martyn P. Chipperfield^{1,2}, Stephen R. Arnold¹, Norbert Glatthor³, Wuhu Feng^{1,4}, Sandip S. Dhomse¹, Brian J. Kerridge⁵, Barry G. Latter⁵, and Richard Siddans⁵

¹School of Earth and Environment, University of Leeds, Leeds, UK

²National Centre for Earth Observation, University of Leeds, Leeds, UK

³Karlsruhe Institute of Technology, Institute of Meteorology and Climate Research, Karlsruhe, Germany

⁴National Centre for Atmospheric Science, University of Leeds, Leeds, UK

⁵Remote Sensing Group, STFC Rutherford Appleton Laboratory, Harwell Oxford, UK

Correspondence: Richard Pope (r.j.pope@leeds.ac.uk)

Received: 2 December 2017 – Discussion started: 18 December 2017

Revised: 5 May 2018 – Accepted: 23 May 2018 – Published: 15 June 2018

Abstract. We have used satellite observations and a simulation from the TOMCAT chemistry transport model (CTM) to investigate the influence of the well-known wintertime North Atlantic Oscillation (NAO) on European tropospheric composition. Under the positive phase of the NAO (NAO-high), strong westerlies tend to enhance transport of European pollution (e.g. nitrogen oxides, NO_x; carbon monoxide, CO) away from anthropogenic source regions. In contrast, during the negative phase of the NAO (NAO-low), more stable meteorological conditions lead to a build-up of pollutants over these regions relative to the wintertime average pollution levels. However, the secondary pollutant ozone shows the opposite signal of larger values during NAO-high. NAO-high introduces Atlantic ozone-enriched air into Europe, while under NAO-low westerly transport of ozone is reduced, yielding lower values over Europe. Furthermore, ozone concentrations are also decreased by chemical loss through the reaction with accumulated primary pollutants such as nitric oxide (NO) in NAO-low. Peroxyacetyl nitrate (PAN) in the upper troposphere–lower stratosphere (UTLS) peaks over Iceland and southern Greenland in NAO-low, between 200 and 100 hPa, consistent with the trapping by an anticyclone at this altitude. Model simulations show that enhanced PAN over Iceland and southern Greenland in NAO-low is associated with vertical transport of polluted air from the mid-troposphere into the UTLS. Overall, this work shows that NAO circulation patterns are an important governing factor for European wintertime composition and air pollution.

1 Introduction

Atmospheric circulation can play an important role in the transport and accumulation of air pollutants from and over source regions (e.g. Pope et al., 2014; Stohl, 2006; Quinn et al., 2007). This is most evident in the Northern Hemisphere winter–spring when emissions of anthropogenic pollutants (e.g. nitrogen oxides, NO_x, and carbon monoxide, CO) are largest (Edwards et al., 2004; Zhou et al., 2012), slower chemical loss mechanisms (i.e. photochemistry and reaction with OH) remove less pollution and wintertime dynamics are enhanced (more intense midlatitude depressions and blocking systems, Trigo, 2006; Hurrell and Deser, 2010). Over North America, the North Atlantic and Europe, the wintertime North Atlantic Oscillation (NAO) is one of the most prominent and frequent modes of atmospheric variability. It represents the redistribution of atmospheric mass between the Arctic and subtropical North Atlantic (Hurrell and Deser, 2010) controlling pressure gradients, wind flows, storm tracks and moisture budgets (Hurrell, 1995; Osborn, 2006). During the NAO positive phase (NAO-high), the climatological Icelandic low and Azores high-pressure systems both intensify, leading to enhanced westerly circulation (storm tracks) across the Atlantic and into north-western Europe. The NAO negative phase (NAO-low) results in a weakening of this meridional pressure gradient leading to reduced westerly winds and a reorientation of the storm tracks over southern continental Europe.

Previous studies have used a range of satellite observations and modelling tools to investigate the impact of NAO circulation patterns on tropospheric composition. Eckhardt et al. (2003) composited Global Ozone Monitoring Experiment (GOME) tropospheric column nitrogen dioxide (TCNO₂) under the wintertime NAO, finding an increase (decrease) of 3–5 (3–7) × 10¹⁴ molecules cm⁻² in the NAO-low (NAO-high) phase over Scandinavia and eastern Europe (UK and France). Thomas and Devasthale (2014), using Atmospheric Infrared Sounder (AIRS) CO at 500 hPa, found that NAO-high and NAO-low significantly increased (2.5 %) and decreased (4 %) CO concentrations over the Nordic countries, respectively. Creilson et al. (2003) investigated the links between the NAO and tropospheric ozone from the Total Ozone Mapping Spectrometer – Solar Backscattered Ultraviolet tropospheric ozone residual (TOR) product (1979–2000). They found the largest correlations between the NAO and TOR in spring, where tropospheric ozone is larger by 3–5 DU (0–2 DU) over central and western Europe (Mediterranean) during the springtime NAO-high (NAO-low). Pausata et al. (2012) found that in December–January–February (DJF) NAO-high significantly increases (90 % confidence level) surface ozone by 6–10 ppbv over the UK and northern Europe, while NAO-low leads to a decrease of 4–10 ppbv. This is indicative of Atlantic ozone-rich air being transported into Europe under a strong westerly flow during NAO-high. Under NAO-low, the weaker winds are reoriented over southern continental Europe aiding the accumulation of primary pollutants (e.g. nitric oxide, NO), which acts as a substantial sink of ozone in winter. Bacer et al. (2016) and Christoudias et al. (2012) used modelled artificial CO and aerosol tracers to find significant negative (positive) correlations between the NAO meteorological fields and composition over Europe (Canada). This highlighted the replacement of European pollution under NAO-high with clean Atlantic air while pollution accumulated over continental Europe during NAO-low.

In this study, we aim to better constrain previously investigated relationships (e.g. NAO–TCNO₂, Eckhardt et al., 2003) and quantify unexplored relationships (e.g. vertical ozone profiles and upper troposphere–lower stratosphere, UTLS; peroxyacetyl nitrate, PAN) between the NAO and atmospheric composition by utilising recent satellite observations with higher spatial resolutions, more frequent sampling and smaller uncertainties (e.g. Ozone Monitoring Instrument (OMI) TCNO₂) and simulations from the TOMCAT chemistry transport model (CTM). These tools allow for a more comprehensive assessment of recent interactions between the NAO and tropospheric composition, the correlation response between trace gases, the extent to which the NAO can influence UTLS composition and an understanding of the key processes governing pollution levels over source regions. Section 2 discusses the observations and model set-up, Sect. 3 describes the links between satellite-observed or model com-

position and the NAO, and our discussion and conclusions are presented in Sects. 4 and 5.

2 Observations and model

2.1 North Atlantic Oscillation Index

Jones et al. (1997) define the North Atlantic Oscillation Index (NAOI) as “the normalised pressure at the southern location (i.e. Gibraltar) minus the normalised pressure at the Icelandic site (i.e. Reykjavik)”. The 2006–2015 wintertime (November–December–January–February, NDJF) NAOI time series (normalised by the time-series standard deviation), obtained from the Climatic Research Unit (CRU), University of East Anglia, is plotted in Fig. 1a. Here, significant NAO-high and NAO-low phases occur when the time series is greater or less than 1.0 and –1.0 standard deviations (blue dotted lines), respectively. However, the multiple satellite records used in this study to assess the composition–circulation relationships all cover different time periods, so the NAO phases are determined based on their corresponding NAOI time series. We then compare the satellite composition–circulation relationships with the model relationships for the 2006–2015 period. Satellite data also have periods of missing data, especially in winter, so the season is extended (i.e. includes November) to build up a sizeable satellite composite for more robust signals.

Figure 1b–e show the pressure anomalies relative to the NDJF 2006–2015 average and winds under both NAO phases at the surface and 10 km derived from European Centre for Medium-Range Weather Forecasts (ECMWF) ERA-Interim data. Under NAO-high (Fig. 1b), the Icelandic low pressure system intensifies by 5–10 hPa at the surface. Over the subtropical North Atlantic, surface pressure increases by 3–5 hPa, yielding a stronger meridional Atlantic pressure gradient. Therefore, enhanced westerly winds (i.e. storm tracks) peaking over 10 m s⁻¹ are orientated over north-western Europe. Green polygon-outlined regions show significant differences (99 % confidence level) between NAO composite pressure and the NDJF average using the Wilcoxon rank test (WRT, Pirovano et al., 2012). NAO-low (Fig. 1c) shows the opposite pattern, with significant positive (negative) pressure anomalies of 5–15 hPa over southern Greenland and Iceland (subtropical North Atlantic). The pressure anomaly reversal yields a weaker meridional pressure gradient, slower easterly winds (below 10 m s⁻¹) between 50 and 60° N and a southwards shift in the storm tracks. At 10 km, the spatial structure and significance of the pressure anomalies are similar to the surface but with smaller absolute differences (i.e. as pressure decreases with altitude). The more uniform westerly flow (Fig. 1d) peaks at approximately 40 m s⁻¹. Under NAO-low (Fig. 1e) the 10 km westerlies are over the subtropical North Atlantic with weakened flow (approximately 10 m s⁻¹) over the mid-North Atlantic.

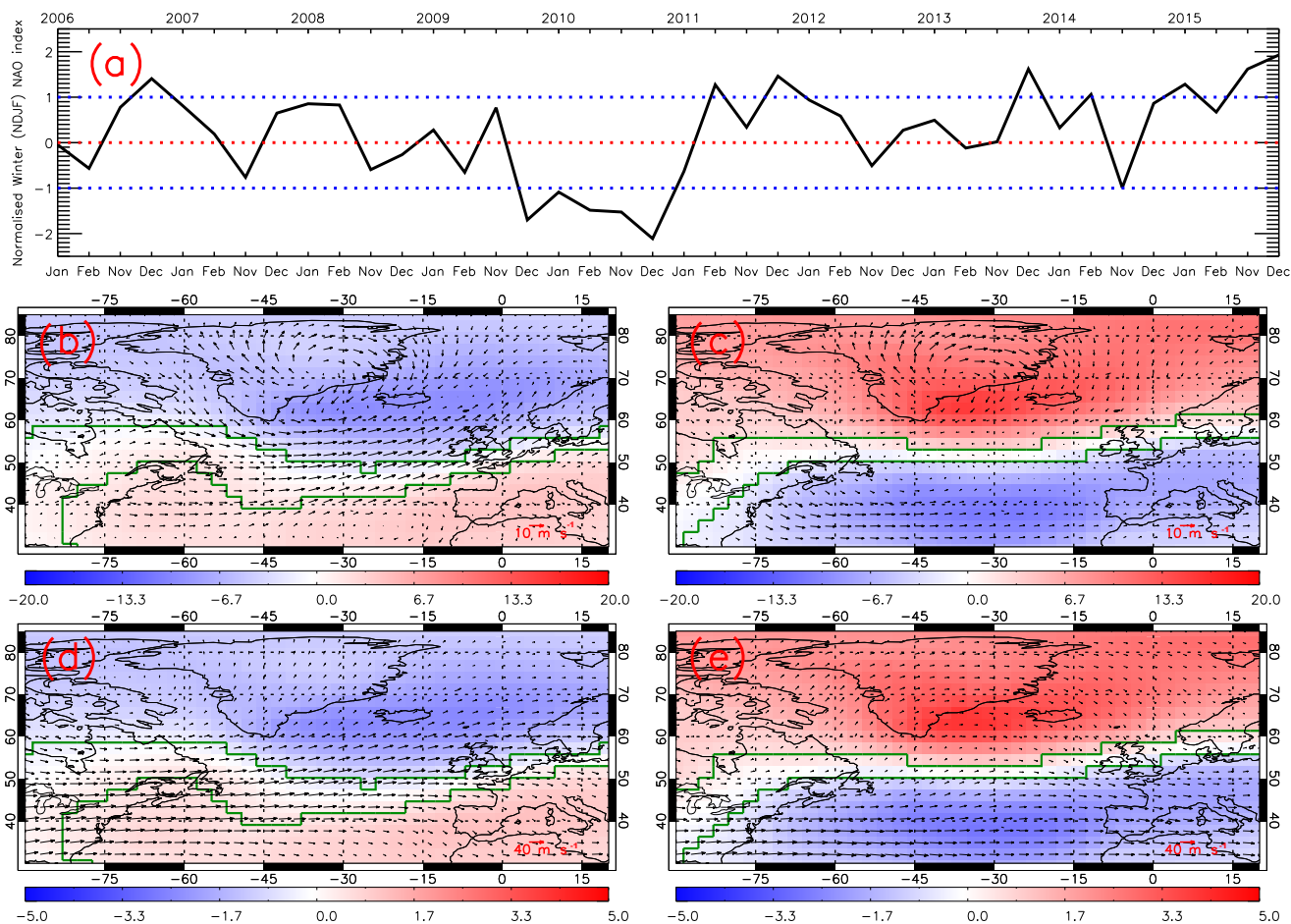


Figure 1. (a) The Climate Research Unit (CRU), University of East Anglia, wintertime (November–December–January–February, NDJF) normalised North Atlantic Oscillation Index (NAOI) from 2006 to 2015. Red and blue lines show the 0 and 1 standard deviation thresholds, where NAOI values outside this range (-1.0 to 1.0 SD) are classed as significant phases. Panels (b) and (c) show the NAO positive and negative-phase surface pressure anomalies (ERA-Interim data) relative to the wintertime average. Panels (d) and (e) show the same as (b) and (c) but for 10 km altitude. Wind vectors are overplotted for the respective NAO phases and altitudes. Green polygon-outlined regions highlight significant differences at the 99 % confidence level based on the Wilcoxon rank test (WRT).

2.2 Satellite observations

To investigate the links between tropospheric composition and the NAO, we have used satellite measurements of TCNO₂, tropospheric ozone profiles (and subcolumns, 0–6 km) and UTLS PAN. TCNO₂ (DOMINO product v2.0; Boersma et al., 2011) from 2005 to 2015 comes from OMI, on board NASA’s AURA satellite (2004–present), with a sun-synchronous overpass of approximately 13.30 local time (LT). OMI is nadir viewing with a spectral range of 270–500 nm and pixel footprint sizes of 16–23 and 24–135 km along and across track, respectively (Boersma et al., 2007). A full description of the OMI NO₂ retrieval is discussed by Eskes and Boersma (2003). Individual retrievals were screened for poor-data-quality flags, geometric cloud fraction greater than 0.2 and the OMI row anomalies (Braak, 2010). We primarily use OMI TCNO₂ data as the instrument

has a much higher spatial resolution and sampling than the GOME TCNO₂ data used by Eckhardt et al. (2003). The OMI TCNO₂ data are also mapped onto a high-resolution $0.05^\circ \times 0.05^\circ$ grid using the pixel-slicing methodology of Pope et al. (2018a). Therefore, we use OMI to build on the work of Eckhardt et al. (2003) and explore whether we can detect a more robust TCNO₂–NAO signal, which is challenging given the short lifetime of NO₂.

Tropospheric ozone measurements used here are from the Tropospheric Emission Spectrometer (TES) on board NASA’s AURA satellite. TES is an infrared Fourier transform spectrometer that measures thermal emissions over the spectral range of $650\text{--}2250\text{ cm}^{-1}$ and has a nadir-viewing footprint of 45 km^2 (Richards et al., 2013). TES has peak sensitivity to lower-tropospheric ozone at approximately 850 hPa (Worden et al., 2013). The TES data have also been

screened for poor-data-quality flags. Previous studies of the NAO impacts on ozone have only used satellite tropospheric column data, either directly or to evaluate model simulations. Therefore, the vertical ozone profiles retrieved by TES provide the opportunity to better understand the vertical response of ozone from NAO circulation patterns.

The Michelson Interferometer for Passive Atmospheric Sounding (MIPAS) operated on board ESA's ENVISAT satellite between 2002 and 2012, and measured many trace gases including PAN in the UTLS. ENVISAT was a sun-synchronous polar-orbiting satellite, which performed 14.4 orbits per day, crossing the equator at about 10:00 and 22:00 LT. MIPAS was a limb-viewing emission spectrometer covering the spectral region between 685 and 2410 cm^{-1} (Fischer et al., 2008), which produced up to 1400 profiles each day. The measurements, in reduced-resolution nominal mode, had 27 tangent altitudes per limb scan. The lowest (uppermost) tangent altitudes ranged approximately from 5 km (70 km) near the poles to 12 km (77 km) at the equator (Wiegele et al., 2012). Few studies have directly used satellite measurements of composition to investigate the influence of the NAO on UTLS trace-gas distributions. This is the first study to use satellite-retrieved UTLS PAN (from the Karlsruhe Institute for Technology (KIT) – see Supplement), which has a lifetime of several months (Singh et al., 1996), to investigate the impact of NAO tropospheric circulation patterns on UTLS composition.

In terms of satellite errors and uncertainties, the random errors are primarily assessed when compositing different chemical species under the two NAO phases. When each chemical species is sampled under the NAO phases and then compared with the seasonal (wintertime) average, the anomalies (i.e. NAO composite – seasonal average) will be dominated by random errors as the systematic errors will cancel out considerably. The averaging of daily data will reduce the random error component by a factor of $1.0/\sqrt{n}$, where n represents the number of days with high-quality satellite data. For example, OMI TCNO₂ n is typically greater than 20–30 observations per grid cell southwards of 60° N, while n ranges between 0 and 10 observations between 60 and 70° N. Therefore, the TCNO₂ signal is less robust northwards of 60° N. The random errors in the different species under both NAO phases is discussed further in the Supplement. However, over the North Atlantic and western Europe, OMI TCNO₂ random errors range between approximately 10 and 40%. For MIPAS PAN at 150 hPa the random errors peak at 15–20% while ranging between 10 and 20% for TES lower-tropospheric ozone. Boersma et al. (2004), Glatthor et al. (2007) and Richards et al. (2008) provided detailed discussion on these product uncertainties.

2.3 TOMCAT 3-D model

TOMCAT is a three-dimensional (3-D) off-line CTM (Chipperfield, 2006). ECMWF ERA-Interim meteorological anal-

yses are used to force the model winds, temperature and humidity (Dee et al., 2011). The standard TOMCAT tropospheric chemistry version uses 82 advected tracers and 229 gas-phase reactions (Emmons et al., 2015), which includes the extended tropospheric chemistry (ExTC) scheme (Monks et al., 2017). TOMCAT also includes heterogeneous N₂O₅ hydrolysis using on-line size-resolved aerosol from the Global Model of Aerosol Processes (GLOMAP) model (Mann et al., 2010). The model anthropogenic emissions come from the Streets v1.2 inventory, which is a composite of several regional emissions inventories (Emmons et al., 2015). The MACCity inventory (Granier et al., 2011) is used for the natural emissions and biomass burning emissions come from the Global Fire Emissions Database (GFED) v3.1 inventory (Randerson et al., 2013). The model was initialised in December 2005, using a restart (initialisation) file from previous simulations, and run for 2006 to 2015 at the $2.8^\circ \times 2.8^\circ$ spatial resolution (Monks et al., 2017). Here, the TOMCAT simulations help to diagnose the key processes governing the satellite-derived NAO–composition relationships by providing information (e.g. the surface) where the satellite instruments cannot detect trace gases and offers full spatial and temporal data coverage.

3 Results

3.1 Observations of tropospheric composition

3.1.1 Nitrogen dioxide

OMI TCNO₂ was sampled under the wintertime (November–February) NAO-high (Fig. 2a) and NAO-low (Fig. 2b) for 2005–2015. Peak TCNO₂ concentrations (over 15×10^{15} molecules cm^{-2}) in both phases are over the Po Valley and the Benelux region. Over the UK, source-region TCNO₂ ranges between 7–13 and 6– 10×10^{15} molecules cm^{-2} in NAO-low and NAO-high. We hypothesise that NAO-high-enhanced westerly flow transports NO₂ off the UK mainland, as seen by Pope et al. (2014), who investigated the impacts of cyclonic conditions on UK TCNO₂. Figure 2c supports this, highlighting significant negative anomalies of -4 to -2×10^{15} molecules cm^{-2} between the TCNO₂ NAO-high composite and 11-year wintertime average. Significant anomalies, shown in the green polygon-outlined regions, are based on the WRT at the 95% confidence level and where composite and wintertime averages \pm their respective random errors (Pope et al., 2015) do not overlap. Systematic errors will cancel when differencing the two TCNO₂ composites. NAO-low reduces westerly flow across Europe and might be expected to aid TCNO₂ accumulation, but there is actually little change in the anomaly field (Fig. 2d). Only the Benelux region ($3\text{--}5 \times 10^{15}$ molecules cm^{-2}) and North Sea (-2.0 to -1.0×10^{15} molecules cm^{-2}) show significant anomalies

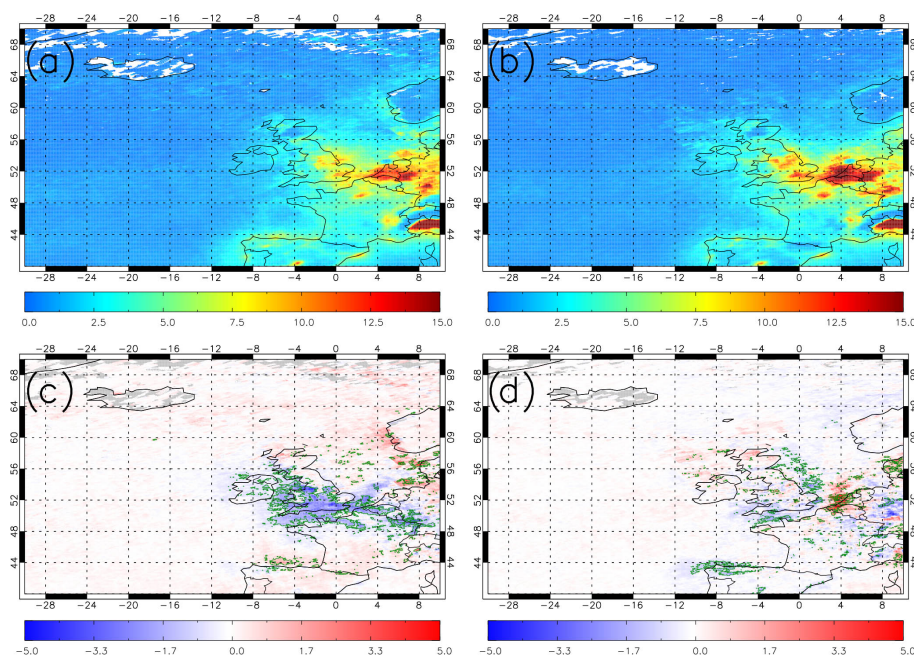


Figure 2. Mean Ozone Monitoring Instrument (OMI) tropospheric column NO_2 (10^{15} molecules cm^{-2}) averaged between 2005 and 2015 under the wintertime (NDJF) NAOI. Panel (a) is column NO_2 sampled under the positive NAO phase, (b) is column NO_2 sampled under the negative NAO phase, (c) shows the column NO_2 positive NAO phase anomaly relative to the wintertime average and (d) is the column NO_2 negative NAO phase anomaly relative to the wintertime average. Green polygon-outlined regions highlight significant differences at the 95 % confidence level based on the WRT.

linked to NO_2 accumulation and reduced transport off the UK mainland.

3.1.2 Peroxyacetyl nitrate

The MIPAS PAN 200–100 hPa average volume mixing ratio, sampled under NAO-high (NDJF) between 2002 and 2012 (Fig. 3a), shows peak (minimum) PAN concentrations of 50–55 (10–20) pptv in the subtropical North Atlantic (over Newfoundland and the Canadian Arctic). During NAO-low (Fig. 3b), PAN concentrations are lower over the subtropical Atlantic but slightly larger over Newfoundland and the Canadian Arctic between 25 and 40 pptv. PAN concentrations are also larger (approximately 40 pptv) over Iceland, southern Greenland and the Denmark Strait, leaving a spatially prominent feature. MIPAS-derived tropopause height (see Supplement) peaks at 11 km in this region, while it is only 9–10 km in the surrounding area (excluding the subtropical North Atlantic). There is also an increase in pressure and convergence of winds over this region (Fig. 1d), potentially highlighting the impact of NAO-low vertical transport of PAN into the UTLS; this is investigated further using TOMCAT (see Sect. 3.2.2). In Fig. 3c under NAO-high, peak significant anomalies of 5–15 pptv occur over the subtropical Atlantic and north-eastern Arctic region (top right of the domain). There are also significant negative anomalies (–15 to –5 pptv) over the Québec region. Significant anomalies are based on the WRT (95 % confidence level)

and where the NAO composite and the wintertime averages plus or minus their uncertainty ranges do not overlap. Over Iceland and Greenland (subtropical North Atlantic and Europe), there are positive (negative) anomalies of 5–15 (–5 to –1) pptv in NAO-low.

Figure 4 shows the zonally averaged ($90\text{--}20^\circ$ E) vertical profiles of MIPAS PAN under the two NAO phases. Peak PAN concentrations at 300–250 hPa range between 100 and 130 pptv in both phases but are larger in NAO-low between 30 and 50° N by 10–20 pptv. However, northwards of 70° N, PAN concentrations between 225 and 100 hPa tend to be larger under NAO-high conditions. Figure 4c shows the NAO-high zonal anomalies relative to the wintertime average (hatched anomalies are insignificant based on the WRT – 95 % confidence level). Northwards of 50° N, significant positive anomalies (5–15 pptv) exist between 300 and 125 hPa. MIPAS-derived tropopause height under NAO-high (see Supplement) is typically higher than in NAO-low over the North Atlantic and Europe by 1–2 km. The higher tropopause signifies enhanced vertical transport, which in this case is the propagation of polluted air masses (i.e. large PAN content) from further down in the troposphere into the UTLS. Southwards of 50° N, positive anomalies occur between 200 and 100 hPa, while negative anomalies are found between 300 and 250 hPa. Under NAO-low conditions (Fig. 4d), there are significant positive anomalies (5–15 pptv) at 300–275 hPa between 30 and 90° N, and they reach up to

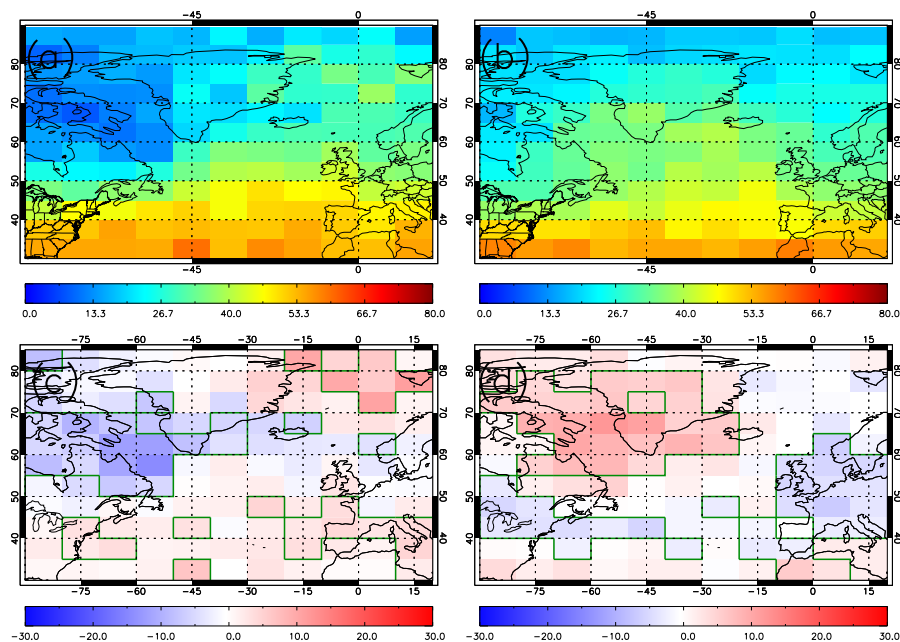


Figure 3. Michelson Interferometer for Passive Atmospheric Sounding (MIPAS) peroxyacetyl nitrate (PAN; pptv) averaged between 200 to 100 hPa for 2002–2012. Panel (a) shows PAN sampled under the wintertime (NDJF) NAO positive phase, (b) shows PAN sampled under the wintertime NAO negative phase, (c) shows the positive NAO phase anomaly relative to the wintertime average and (d) shows the negative NAO phase anomaly relative to the wintertime average. Green polygon-outlined regions highlight significant differences at the 95 % confidence level based on the WRT.

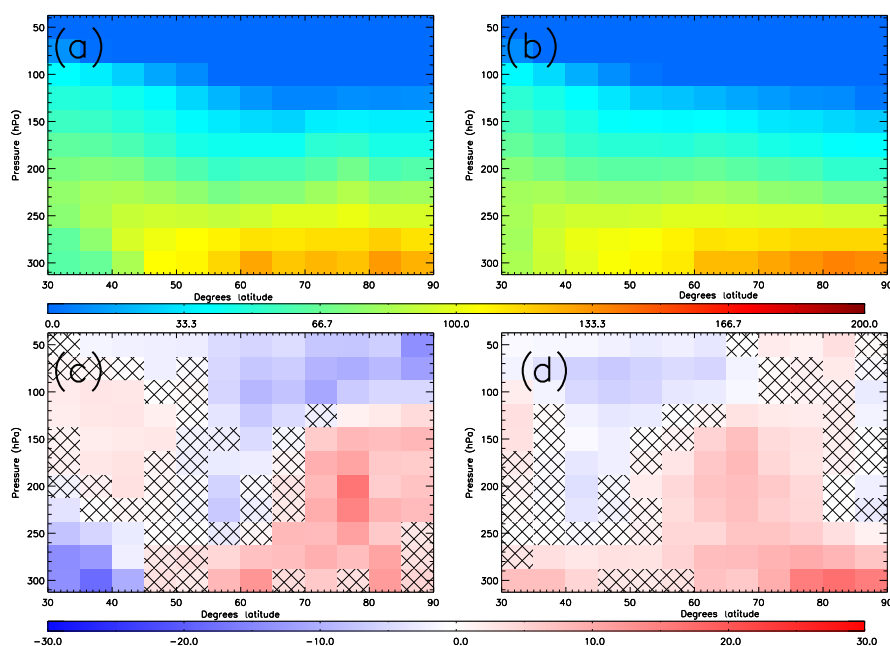


Figure 4. MIPAS PAN (pptv), 2002–2012, zonally averaged (90° W to 20° E) for (a) the wintertime (NDJF) NAO positive phase, (b) the wintertime NAO negative phase, (c) the positive NAO phase anomaly relative to the wintertime average and (d) the negative NAO phase anomaly relative to the wintertime average. Black hatched regions highlight insignificant differences at the 95 % confidence level based on the WRT.

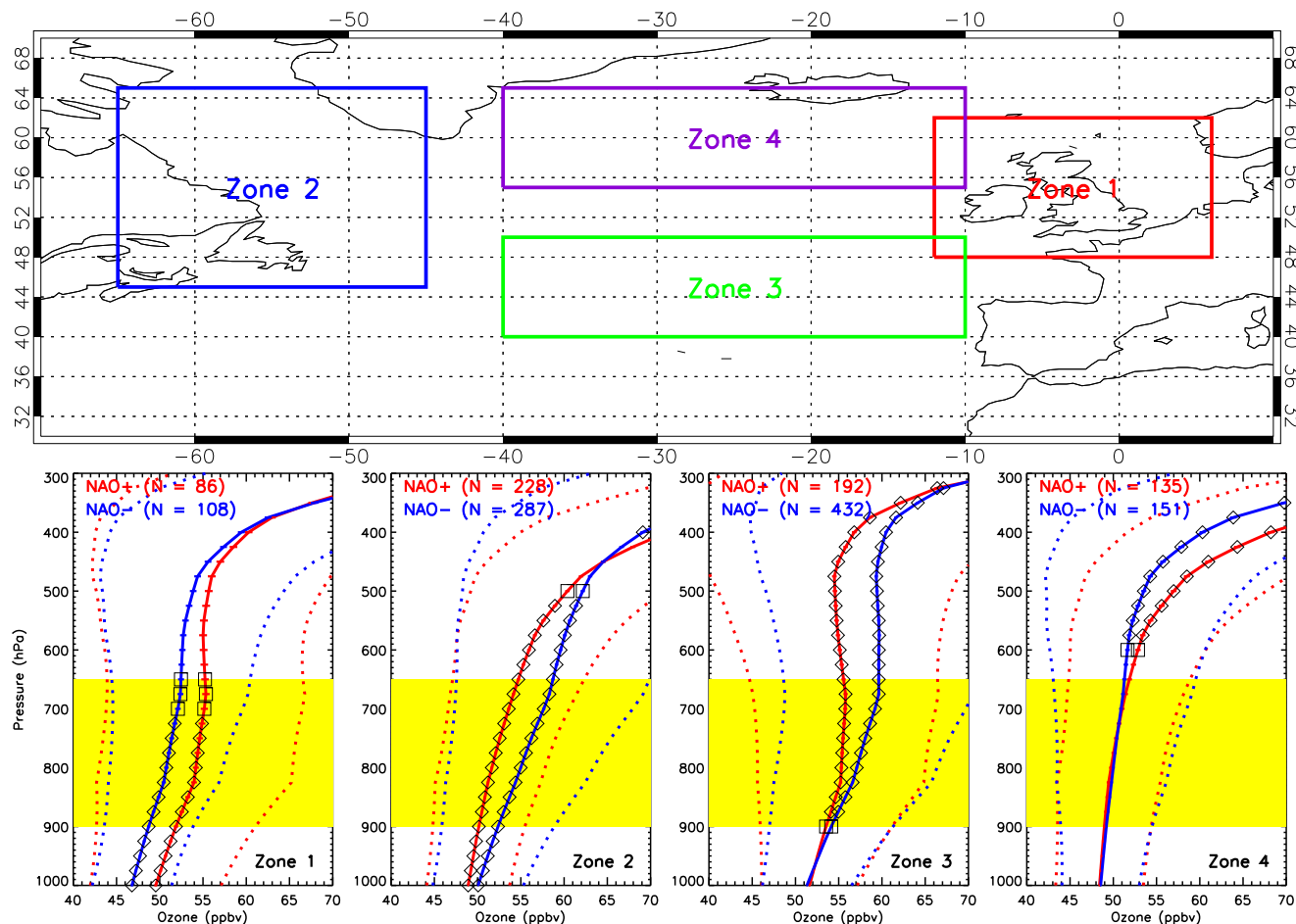


Figure 5. Tropospheric Emission Spectrometer (TES) ozone profiles, averaged over four regions (Zone 1: 48–62° N, 12° W–6° E; Zone 2: 45–65° N, 45–65° W; Zone 3: 40–50° N, 10–40° W; Zone 4: 55–65° N, 10–40° W), between 2005 and 2011, sampled under the winter-time (NDJF) NAO positive (red line) and negative (blue line) phases. Horizontal lines show the satellite uncertainty range, the yellow box highlights the region of peak TES sensitivity to lower-tropospheric ozone and the dotted lines show the profile averages are plus or minus their respective standard deviations. Squares and diamonds show where the ozone profiles sampled under each NAO phase are significantly different from each other at the 90 and 95 % confidence levels based on the WRT.

125 hPa at 60–80° N coinciding with peak PAN concentrations over Iceland in Fig. 3b. Significant negative anomalies (–5 to –1 pptv) exist at 225–50 hPa, which coincides with the negative anomalies in Fig. 3d over the subtropical Atlantic. Between 30 and 50° N, there is an altitude anomaly dipole reversal with NAO-high showing significant positive (negative) anomalies at 200–100 hPa (300–250 hPa) and NAO-low highlighting significant positive (negative) anomalies at 300–275 hPa (225–50 hPa). These patterns are linked to changes to regional circulation patterns under the different NAO phases and will be explored further using TOMCAT in Sect. 3.2.2.

3.1.3 Ozone

Figure 5 shows TES vertical profiles averaged over four regions (Zones 1–4) covering the North Atlantic between 2005

and 2011, which were sampled during significant winter-time (November–February) NAO events. These four domains are selected because TES has infrequent spatial sampling (Richards et al., 2008) meaning spatial ozone distributions are often noisy or unclear. In Zone 1 (UK), TES ozone sampled under NAO-high (red line) is significantly larger (90 % – squares and 95 % – diamonds) than in NAO-low (blue line) by 3–4 ppbv throughout the region of peak sensitivity (900–650 hPa – yellow box). Similar patterns exist in surface ozone measurements from the UK Automatic Urban and Rural Network (AURN, DEFRA, 2015). Under NAO-high, surface ozone concentrations were significantly higher than in NAO-low by 5–10 $\mu\text{g m}^{-3}$ across the UK (see Supplement). The opposite is true for AURN surface NO_2 where concentrations across the UK are lower by 5–10 $\mu\text{g m}^{-3}$ in NAO-high. This supports the hypothesis that NAO-high increases (decreases) ozone concentrations over western Europe (west-

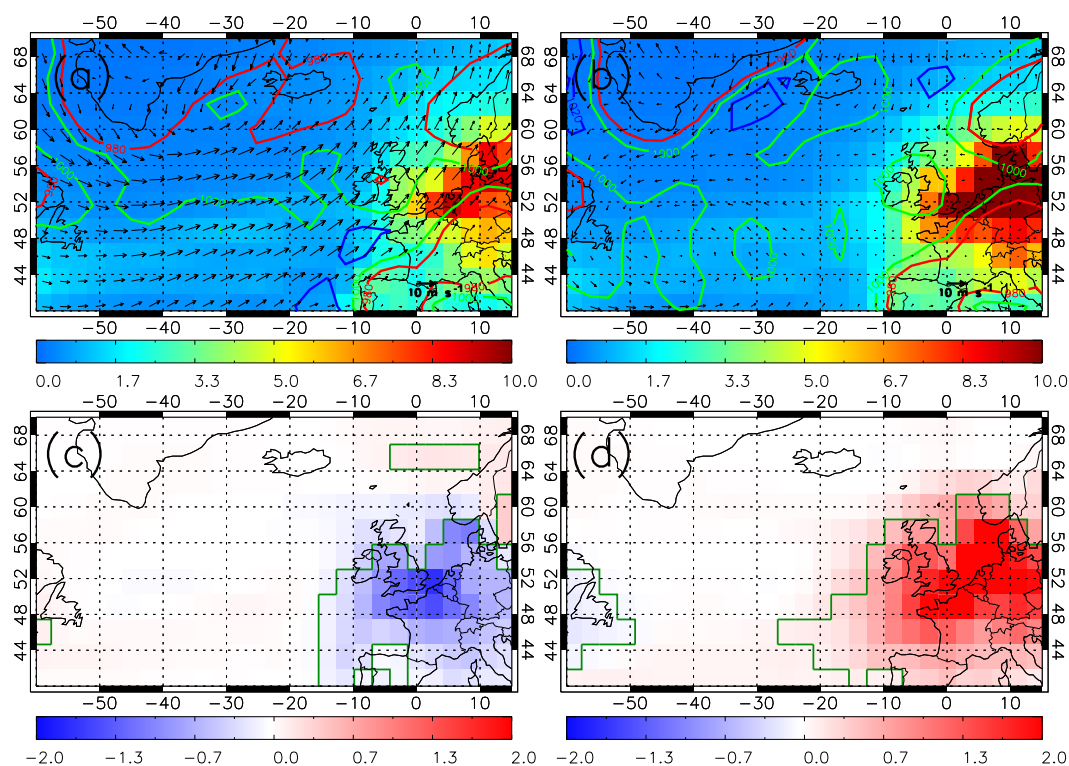


Figure 6. TOMCAT troposphere column NO_2 (10^{15} molecules cm^{-2}) averaged between 2006 and 2015 sampled under the wintertime (NDJF) NAO. Panel (a) NAO positive phase, (b) NAO negative phase. (c) shows the NAO positive phase anomaly relative to the wintertime average and (d) shows the negative NAO phase anomaly relative to the wintertime average. Wind vectors show the horizontal 10 m winds and the red, green and blue contours represent 980, 1000 and 1020 hPa surface pressure. Green polygon-outlined regions in (c) and (d) highlight significant differences at the 95 % confidence level based on the WRT.

ern Atlantic) through enhanced westerly transport of ozone and dispersion of other species involved in its removal (e.g. NO) over Europe. Zone 2 (Newfoundland) has the opposite signal whereby the NAO-low ozone profile is significantly (95 %) larger than the NAO-high profile by 2–4 ppbv. Again, this is potentially linked to enhanced westerly ozone transport across the Atlantic towards Europe during NAO-high. In Zone 3 (North Atlantic), there are insignificant differences at approximately 900 hPa. However, ozone is significantly greater under NAO-low between 875 and 350 hPa. There are insignificant differences in Zone 4 ozone up to 600 hPa, but NAO-high ozone is significantly larger above this altitude.

3.2 Model results

TOMCAT has been evaluated in multiple studies (e.g. Monks et al., 2017; Richards et al., 2013) for NO_2 , PAN and ozone, which are discussed in detail in the Supplement. We also have evaluated TOMCAT surface and tropospheric ozone against a range of observations covering western Europe and the North Atlantic. In all cases, TOMCAT can suitably represent these chemical tracers and their responses to the NAO circulation patterns (see Supplement).

3.2.1 Nitrogen dioxide

In NAO-high and NAO-low (Fig. 6a and b), where TOMCAT has been sampled under the NAO phases in Fig. 1a, the model TCNO_2 over western Europe ranges between 3 and 9×10^{15} molecules cm^{-2} and 6 to over 10×10^{15} molecules cm^{-2} . Over the UK, NAO-high-enhanced westerly flow transports NO_2 off the mainland (Fig. 6c) with significant negative anomalies of -2.0 to -0.5×10^{15} molecules cm^{-2} relative to the wintertime average. OMI TCNO_2 has a similar NAO-high UK signal (2c), but it is less spatially extensive and does not cover as much of continental Europe. In NAO-low, OMI (Fig. 2d) only shows accumulation of TCNO_2 over the Benelux region, while TOMCAT (positive anomalies over 1.5×10^{15} molecules cm^{-2}) accumulates TCNO_2 over all of continental Europe (Fig. 6d). Potential reasons for model-satellite NAO-low anomaly differences (Fig. 2d and 6d) included the following. (1) As OMI has peak retrieval sensitivity in the middle–upper troposphere it potentially underestimates the full TCNO_2 under NAO-low conditions when the more stable conditions trap NO_2 in the boundary layer. (2) The model NO_2 lifetime in the NAO-low composite is

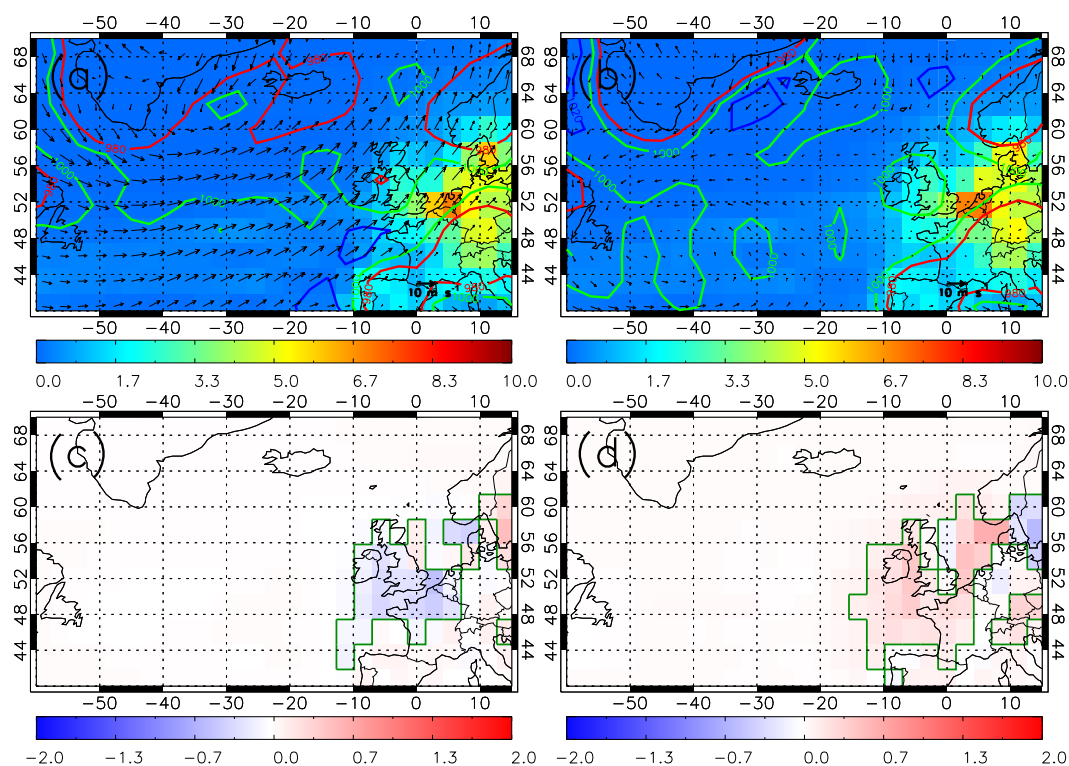


Figure 7. TOMCAT surface NO_2 (ppbv) averaged between 2006 and 2015 sampled under the wintertime (NDJF) NAO. Panel (a) NAO positive phase, (b) NAO negative phase, (c) shows the NAO positive phase anomaly relative to the wintertime average and (d) shows the negative NAO phase anomaly relative to the wintertime average. Wind vectors show the horizontal 10m winds and the red, green and blue contours represent 980, 1000 and 1020 hPa. Green polygon-outlined regions in (c) and (d) highlight significant differences at the 95 % confidence level based on the WRT.

potentially longer than the satellite equivalent as it represents all-sky conditions, while the satellite composite represents clear-sky conditions only (i.e. more photochemical loss of NO_2).

At the surface, TOMCAT surface NO_2 ranges between 0–6 and 2–8 ppbv in NAO-high and NAO-low. TOMCAT does have a systematic surface NO_2 low bias against surface observations (see Supplement), but this systematic offset is removed when considering anomalies (Fig. 8c and d) relative to the wintertime average. TOMCAT surface anomalies typically have similar spatial patterns to the TOMCAT TCNO_2 , but they are less spatially extensive. Under the NAO-high, there are significant negative (positive) anomalies of -0.5 (0.2) ppbv over the UK (North Sea), highlighting the westerly transport of NO_2 off the UK mainland. Under NAO-low, significant positive anomalies (0.0 to 1.0 ppbv) highlight the accumulation of NO_2 from reduced westerly flow across the UK. This is consistent with the AURN results presented in the Supplement. The model also shows a significant anomaly dipole over Scandinavia which reverses between phases. This, in combination with the reduced spatial impact on surface NO_2 compared with the tropospheric pattern, implies that processes above the surface also influ-

ence the response of the tropospheric NO_2 distribution to the NAO.

Figure 8 shows the TOMCAT NO_2 meridional vertical cross section at 0° E. Between 35 and 60° N TOMCAT simulates NO_2 concentrations above 1.0 ppbv from 1000 hPa to 900 (850) hPa in NAO-high (NAO-low). Negative anomalies (under -0.05 ppbv) relative to the wintertime average from 1000 to 900 hPa at 50° N (Fig. 8c), show the enhanced NAO-high westerly flow transporting NO_2 throughout the boundary layer away from UK source regions. This NO_2 is transported into the North Sea, yielding positive anomalies of 0.02 ppbv northwards of 55° N with vertical ascent into the mid-troposphere (approximately 600–700 hPa at 60 – 70° N). Under NAO-low (Fig. 8d), there are positive (above 0.05 pptv) anomalies between 35 and 65° N as the weakened meridional winds have a southerly flow with ascent (descent) at 65 (40) $^\circ$ N. This highlights reduced NO_2 transport from the climatological westerlies aiding accumulation in the lower troposphere (1000–700 hPa). Therefore, processes throughout the lower troposphere over the UK are important in governing the tropospheric column burden during the two NAO phases.

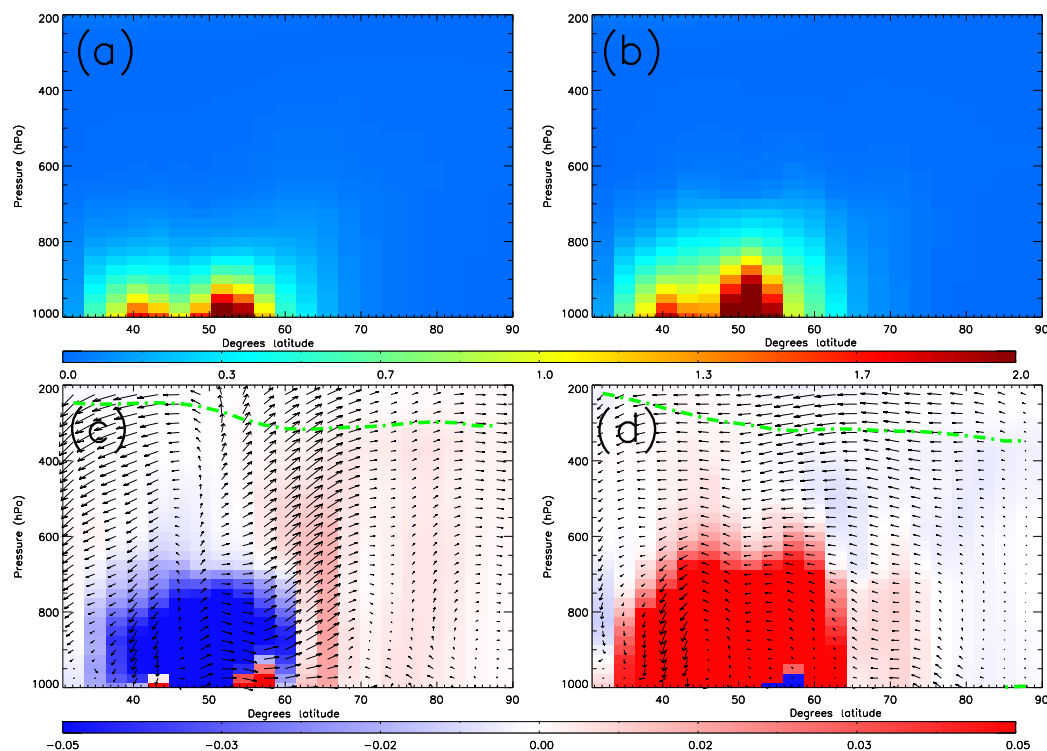


Figure 8. TOMCAT NO_2 (ppbv) cross section at 0° E averaged between 2006 and 2015 sampled under the wintertime (NDJF) NAO. (a) NAO positive phase, (b) NAO negative phase, (c) shows the NAO positive phase anomaly relative to the wintertime average and (d) shows the negative NAO phase anomaly relative to the wintertime average. Green dashed lines represents the dynamical tropopause. Wind vectors represent the cross section (0° E) meridional and vertical (scaled by 10^4) winds.

3.2.2 Peroxyacetyl nitrate

At the surface, although PAN has lower concentrations than NO_2 in source regions, it has a longer lifetime resulting in more significant responses to the seasonal average under the different NAO phases. Under NAO-high (Fig. 9a), TOMCAT surface PAN peaks between 200 and 220 pptv over the western Atlantic. Over Europe, PAN ranges between 150 and 170 pptv as, like NO_2 , enhanced westerly flow transports PAN away from western European source regions, replacing it with cleaner subtropical North Atlantic air (100–150 pptv). Through reduced transport, NAO-low conditions aid pollutant accumulation over continental Europe with PAN concentrations of 190 to over 300 pptv. The NAO-high TOMCAT PAN anomalies (Fig. 9c) relative to the wintertime average highlight reduced concentrations of -50 to -20 pptv over continental Europe, while in the western North Atlantic there are no significant anomalies. This infers similar transport processes to the wintertime average, resulting in minimal PAN changes, yet NAO-low (Fig. 9d) weakens or reverses the winds, yielding significant negative anomalies of -20 to -10 pptv. Therefore, westerly flow, similar under NAO-high and average wintertime conditions, aids the long-range transport of PAN from North America. As NAO-low inter-

rupts this transport pathway, there is a significant decrease in background PAN.

We now investigate whether TOMCAT reproduces the MIPAS UTLS PAN patterns under the NAO phases, despite the slightly different time periods. Previous studies (e.g. Emmons et al., 2015; Pope et al., 2016) have shown that TOMCAT PAN compares reasonably well with aircraft observations, but there is a systematic difference between TOMCAT and KIT MIPAS PAN (see Supplement). Therefore, we primarily focus on the anomalies relative to the wintertime average under the NAO phases, as this systemic difference is removed. TOMCAT PAN 200–100 hPa average peaks (over 50 pptv) in NAO-high over the western subtropical North Atlantic (Fig. 10a). The south-westerly flow (approximately 30 m s^{-1}) at this altitude transports PAN across the Atlantic, reaching 35 pptv over Iberia. However, at approximately 0° E, a southerly shift in the winds over the Mediterranean leads to lower continental Europe PAN concentrations (20–30 pptv). Northwards of 70° N, the flow ($20\text{--}30 \text{ m s}^{-1}$) accumulates PAN over the Arctic region (20–24 pptv). Similar spatial patterns are seen in MIPAS with peak PAN concentrations over the western subtropical Atlantic, minimum PAN over Canada and Hudson Bay and elevated PAN in the Arctic region. However, MIPAS PAN absolute concen-

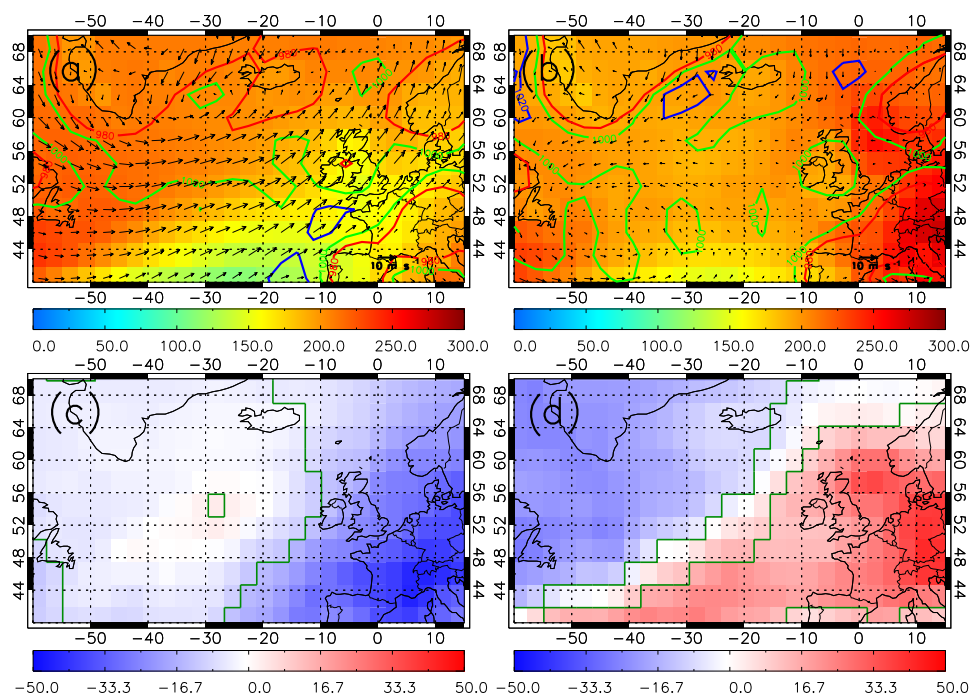


Figure 9. TOMCAT surface PAN (pptv) averaged between 2006 and 2015 sampled under the wintertime (NDJF) NAO. Panel (a) NAO positive phase, (b) NAO negative phase, (c) shows the NAO positive phase anomaly relative to the wintertime average and (d) shows the negative NAO phase anomaly relative to the wintertime average. Wind vectors show the horizontal 10 m winds and the red, green and blue contours represent 980, 1000 and 1020 hPa surface pressure. Green polygon-outlined regions in (c) and (d) highlight significant differences at the 95 % confidence level based on the WRT.

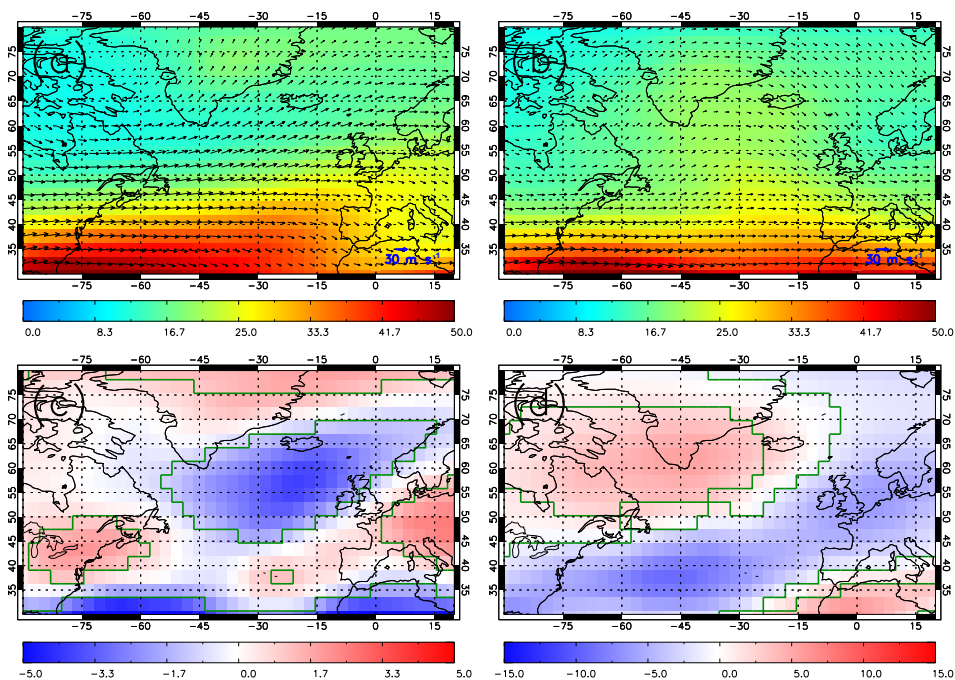


Figure 10. TOMCAT PAN (pptv) averaged between 200 and 100 hPa for 2006–2015 sampled under the wintertime (NDJF) NAO. Panel (a) NAO positive phase, (b) NAO negative phase, (c) shows the NAO positive phase anomaly relative to the wintertime average and (d) shows the negative NAO phase anomaly relative to the wintertime average. Wind vectors show the horizontal 200–100 hPa winds. Green polygon-outlined regions in (c) and (d) highlight significant differences at the 95 % confidence level based on the WRT.

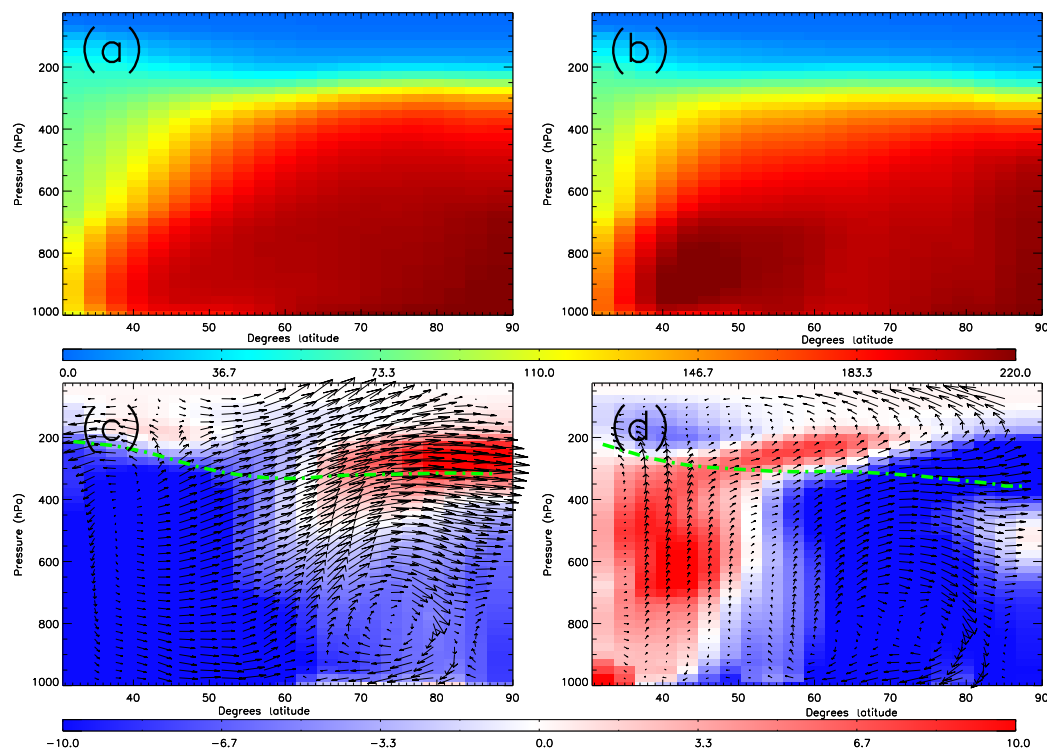


Figure 11. TOMCAT zonally averaged (90° W to 20° E) PAN (pptv) between 2006 and 2015 sampled under the wintertime (NDJF) NAO. Panel (a) NAO positive phase, (b) NAO negative phase, (c) shows the NAO positive phase anomaly relative to the wintertime average and (d) shows the negative NAO phase anomaly relative to the wintertime average. Green dashed lines represents the dynamical tropopause. Wind vectors represent the zonally averaged (90° W to 20° E) meridional and vertical (scaled by 10^4) winds.

trations are systematically higher than TOMCAT (see Supplement). Vertical transport will also have an important impact on NAO-high, as signified by the higher MIPAS-derived tropopause height (see Supplement), with propagation of polluted air masses from the lower troposphere into the UTLS. In NAO-low, peak PAN (over 40 ppbv) occurs in the subtropical Atlantic where the winds are predominately zonal (westerly), yielding lower PAN concentrations (15–25 pptv) over the mid-North Atlantic. Continental Europe PAN concentrations decrease (10–20 pptv), as north-westerly flow transports cleaner Arctic air masses into the region. PAN accumulation over Iceland and southern Greenland (25 ppbv) correlates with the large UTLS pressure increase shown in Fig. 1d. Figure 10d highlights the significant enhancement of PAN over Iceland and southern Greenland with positive anomalies relative to the wintertime average of 5–10 pptv. Again, the MIPAS-derived tropopause height in NAO-low peaks in this region (approximately 11 km – see Supplement) suggesting sufficiently strong vertical transport of tropospheric air masses. In NAO-low, as the strong westerly flow in NAO-high (Fig. 10b) has shifted equatorwards, there are significant negative anomalies under -15 pptv across the North Atlantic, which match the MIPAS equivalent in Fig. 3d. There are some similarities between the TOMCAT (Fig. 10c) and

MIPAS (Fig. 3c) NAO-high PAN anomalies with increased PAN in the eastern Arctic. However, TOMCAT simulates positive anomalies (0–5 pptv) over the North Atlantic between 35 and 45° N, while MIPAS has significant positive anomalies of 10 pptv. TOMCAT also simulates significant negative anomalies over the UK and the eastern North Atlantic, which are not observed by MIPAS. Therefore, the model results only allow for limited assessment of the NAO influence of UTLS PAN in NAO-high over these regions.

Figure 11 shows the zonal average (90° W– 20° E) meridional-vertical TOMCAT PAN distribution under both NAO phases. Between 1000 and 600 hPa, PAN concentrations are above 200 pptv apart from in the region 30 – 40° N. From 400 to 200 hPa, there is a sharp PAN decrease to less than 30 pptv. The vertical PAN profile between 30 and 40° N differs from other latitude bands, with PAN peaking at 150–200 pptv from 1000 to 700 hPa and then from 60–100 pptv up to 200 hPa. Between 200 and 100 hPa, PAN concentrations (30–60 pptv) are larger than other latitude bands linked to the higher tropopause (also observed by MIPAS – see Supplement). The significant decreases in surface PAN over Europe from NAO-high enhanced westerly flow (Fig. 9c) occur throughout the troposphere, with negative zonal anomalies of -10 to -3 pptv (Fig. 11c). Above the tropopause

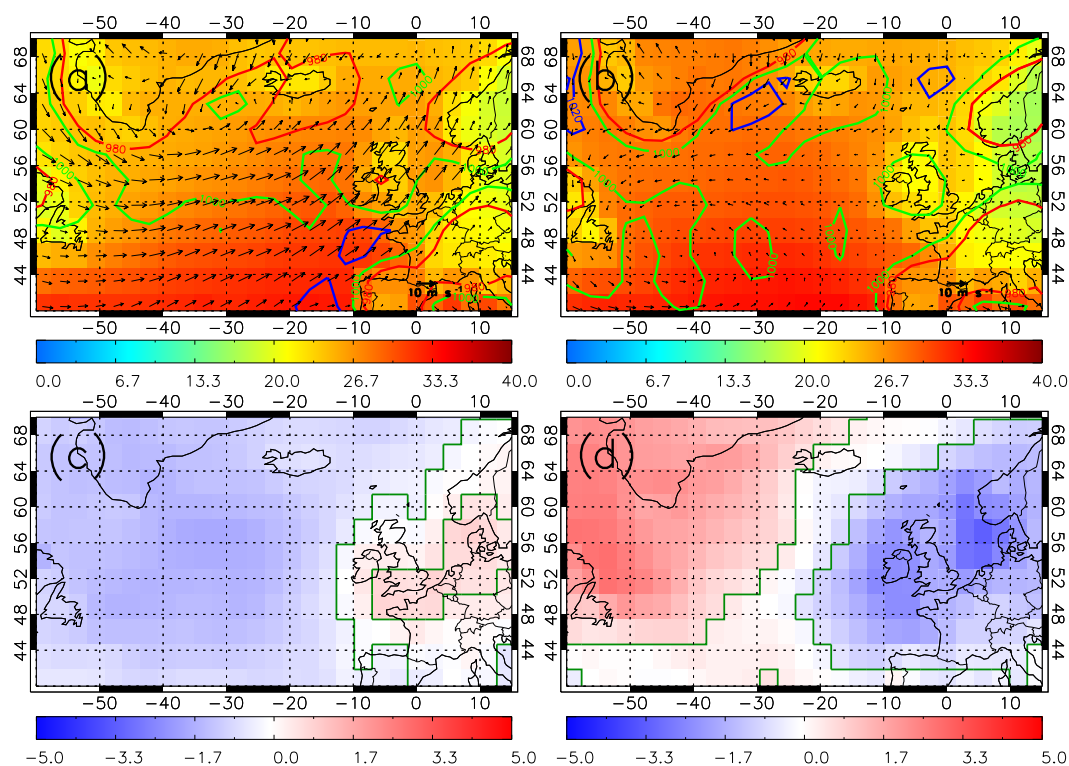


Figure 12. TOMCAT surface ozone (ppbv) averaged between 2006 and 2015 sampled under the wintertime (NDJF) NAO. Panel (a) NAO positive phase, (b) NAO negative phase, (c) shows the NAO positive phase anomaly relative to the wintertime average and (d) shows the negative NAO phase anomaly relative to the wintertime average. Wind vectors show the horizontal 10 m winds and the red, green and blue contours represent 980, 1000 and 1020 hPa surface pressure. Green polygon-outlined regions in (c) and (d) highlight significant differences at the 95 % confidence level based on the WRT.

(dashed green line), strong vertical (winds are scaled by 10^4 for clarity) meridional transport accumulates PAN (positive anomalies over 10 pptv) in the Arctic UTLS. Under NAO-low (Fig. 11d), there are positive (5–10 pptv) and negative (–10 to –5 pptv) anomalies between 30–50 and 60–90° N throughout the troposphere. The surface patterns (Fig. 9d), where reduced transport aids PAN accumulation over Europe, appear to account for this zonal tropospheric pattern. Between 30 and 50° N, there is limited meridional flow aiding PAN accumulation over Europe in NAO-low. The vertical flow contributes to positive anomalies (3–5 pptv) propagating into the UTLS, which is consistent with the PAN accumulation shown in Fig. 10d between 50 and 70° N.

3.2.3 Ozone

TOMCAT surface ozone under NAO-high (Fig. 12a) peaks at approximately 28–30 ppbv over the subtropical and western North Atlantic co-located with the enhanced westerlies. Over continental Europe, ozone concentrations are significantly larger (1–2 ppbv – Fig. 12c) than the wintertime average, ranging between 16 and 25 ppbv. This matches a similar pattern in the observations: AURN surface ozone was significantly higher over the UK under NAO-high than NAO-

low (see Supplement), and TES lower-tropospheric ozone (Zone 1, Fig. 5) was larger under NAO-high. In Zone 2, TES lower-tropospheric ozone was higher under NAO-low, which correlates with the surface TOMCAT pattern. Pausata et al. (2012) found similar patterns with significant positive (negative) correlations over Europe (western North Atlantic) between surface ozone and the NAOI in DJF. Under NAO-low conditions, TOMCAT ozone concentrations are consistent across the North Atlantic (28–30 ppbv) as the weakened or reversed westerlies limit the transport of ozone-enriched Atlantic into Europe yielding lower concentrations of 13–20 ppbv. Over the western North Atlantic (Europe), ozone concentrations (Fig. 12d) have increased (decreased) with significant positive (negative) anomalies of 2–3 ppbv (–3 to –1 pptv). Again, Pausata et al. (2012) presented similar results which also match TES and AURN ozone observations (see Supplement). TOMCAT tropospheric column ozone (not shown here) also showed similar anomalies.

At the surface, the PAN and NO_2 spatial anomalies are anti-correlated with ozone, so UTLS ozone (Fig. 13) was investigated to see if this relationship was consistent at higher altitudes. TOMCAT 200–100 hPa average ozone, sampled under NAO-high, ranges from 800 to 1000 ppbv northwards

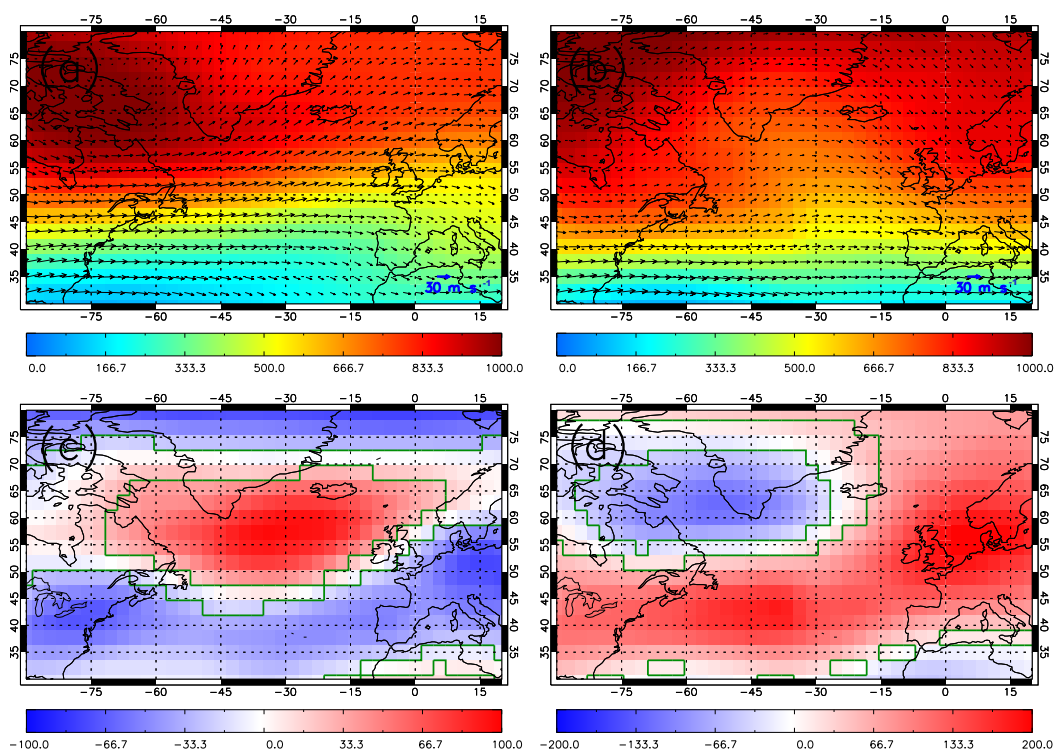


Figure 13. TOMCAT ozone (ppbv) averaged between 200 and 100 hPa for 2006–2015 sampled under the wintertime (NDJF) NAO. Panel (a) NAO positive phase, (b) NAO negative phase, (c) represents the NAO positive phase anomaly relative to the wintertime average and (d) represents the negative NAO phase anomaly relative to the wintertime average. Wind vectors show the horizontal 200–100 hPa winds. Green polygon-outlined regions in (c) and (d) highlight significant differences at the 95 % confidence level based on the WRT.

of 60° N but decreases towards the subtropical North Atlantic with minimum concentrations of 150–200 ppbv. A similar pattern occurs under NAO-low except for the ozone-reduced air mass (500–700 pptv), stretching from approximately 45 to 65° N along 15–45° W. Higher ozone concentrations (800–1000 ppbv) also propagate further south in NAO-low on either side of the Atlantic, surrounding the reduced ozone limb. The UTLS ozone anomalies (Fig. 13c and d) are also anti-correlated with the PAN. Whereas PAN has positive anomalies across the Atlantic basin in NAO-high, there are significant negative ozone anomalies (under -100 ppbv). This anti-correlation is also prominent under NAO-low, where significant TOMCAT ozone anomalies (50–200 ppbv) exist over the mid-North Atlantic and Europe but are significantly negative for PAN. As shown in Figs. 10 and 11, tropospheric positive PAN anomalies propagate into the UTLS over Iceland and southern Greenland, but the ozone anomalies are significantly negative (-150 to -50 ppbv). Potential reasons for the PAN-ozone anti-correlation include the air mass origin or the PAN (NO_x)-ozone chemistry. The thermal decomposition of PAN forms the peroxyacetyl radical and NO_2 , which is an UTLS ozone sink (i.e. conversion of NO_2 to NO and then reaction with ozone), while a tropospheric ozone source is in the presence of volatile organic compounds

(Richards et al., 2013). However, lower UTLS temperatures (i.e. around 250 K) yield a PAN lifetime of several months (Singh, 1987) and are a less likely factor in the PAN NO_x -ozone anomaly anti-correlations. Cohen et al. (1994) show that UTLS ozone- HO_x chemistry is a more significant sink pathway for ozone; however, there is no clear correlation between the NAO HO_2 and ozone anomalies. Methane, a good air mass tracer due to its approximate 9-year lifetime (e.g. McNorton et al., 2016) and anthropogenic source, was sampled under the NAO phases (not shown) and highlighted similar anomaly patterns to PAN, again anti-correlated with ozone. Therefore, PAN and methane (ozone) act as signatures for the transport of polluted (clean) air masses in the troposphere for the different NAO phases.

Figure 14 shows the TOMCAT ozone cross section at 0° E, similar to NO_2 in Fig. 8. Under both NAO phases, lower-tropospheric (UTLS – above 300 hPa) ozone ranges between 25 and 35 (above 100) ppbv. Meridionally, there is a decreasing poleward lower-tropospheric ozone gradient, while in the UTLS peak (minimum) concentrations are at the pole (30° N). The anomalies, as discussed above, are anti-correlated with NO_2 . In NAO-high, there are small positive (negative) anomalies over the UK (North Sea) consistent with ozone-enriched air transported into the UK from

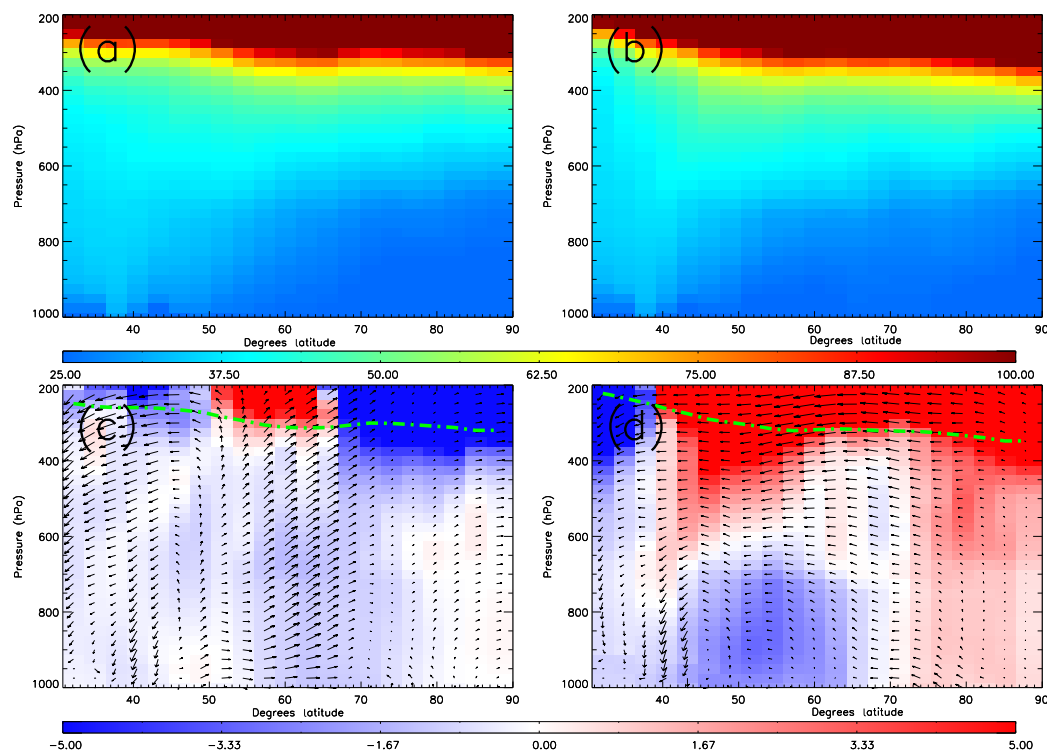


Figure 14. TOMCAT ozone (ppbv) cross section at 0° E averaged between 2006 and 2015 sampled under the wintertime (NDJF) NAO. Panel (a) NAO positive phase, (b) NAO negative phase, (c) shows the NAO positive phase anomaly relative to the wintertime average and (d) shows the negative NAO phase anomaly relative to the wintertime average. Green dashed lines represents the dynamical tropopause. Wind vectors represent the cross section (0° E) meridional and vertical (scaled by 10^4) winds.

the North Atlantic and ozone loss downwind due to source-region NO_x transport, which propagates up to approximately 600 hPa. The positive anomalies in the UTLS at 60° N are consistent with ozone accumulation seen in Fig. 13. Under NAO-low conditions, the negative anomalies (approximately -3 ppbv) between 45 – 65° N and 1000 – 700 hPa are linked to UK NO_x accumulation (Fig. 7d). Atmospheric downwelling leads to UTLS ozone (positive anomalies over 3 ppbv) propagation into the mid-troposphere at 40 – 50° N. At high latitudes, small positive anomalies throughout the troposphere, which are anti-correlated with PAN, show clean-air transport around the UTLS Icelandic–southern Greenland anticyclone in which PAN accumulates.

A second TOMCAT ozone cross section at 56.25° W (Fig. 15) has similar absolute ozone concentrations to the 0° E cross sections, but the anomalies highlight important differences. In NAO-high, both cross sections have similar lower-tropospheric ozone anomalies except at 50° N (Figs. 14c and 15c) with positive anomalies (approximately 1 ppbv) over the UK region and near 0 ppbv over the western North Atlantic. Under NAO-low conditions, there are positive anomalies (Fig. 15d, 1–3 ppbv) between 1000 – 600 hPa and 50 – 70° N, but the eastern cross section (Fig. 14d) highlights negative anomalies in this region (-3 to -1 pptv).

While there is downwelling of stratospheric ozone in the eastern cross section into the middle–upper troposphere during NAO-low, the western cross section has an upwelling of ozone-reduced air into the UTLS with negative anomalies of less than -5 ppbv. Overall, in the lower troposphere, the TOMCAT cross section anomalies support the signals in the TES data. Over the UK (Zone 1, Fig. 5, and eastern cross section, Fig. 14), lower-tropospheric ozone is larger (lower) than the wintertime average under NAO-high (NAO-low), while the opposite occurs in the western North Atlantic (Zone 2 and western cross section, Fig. 15).

4 Discussion

The analysis of satellite-observed and model-simulated atmospheric composition sampled under the different wintertime NAO phases clearly highlights the importance of transport, both horizontal and vertical, for variability in concentrations of the air pollutant species investigated. At the surface and in the lower troposphere, enhanced westerly flow in NAO-high influences primary pollutant concentrations (e.g. NO_2) over Europe as they are transported away from source regions and replaced by clear Atlantic air masses. As NO_2 has a short lifetime of several hours, there is little impact

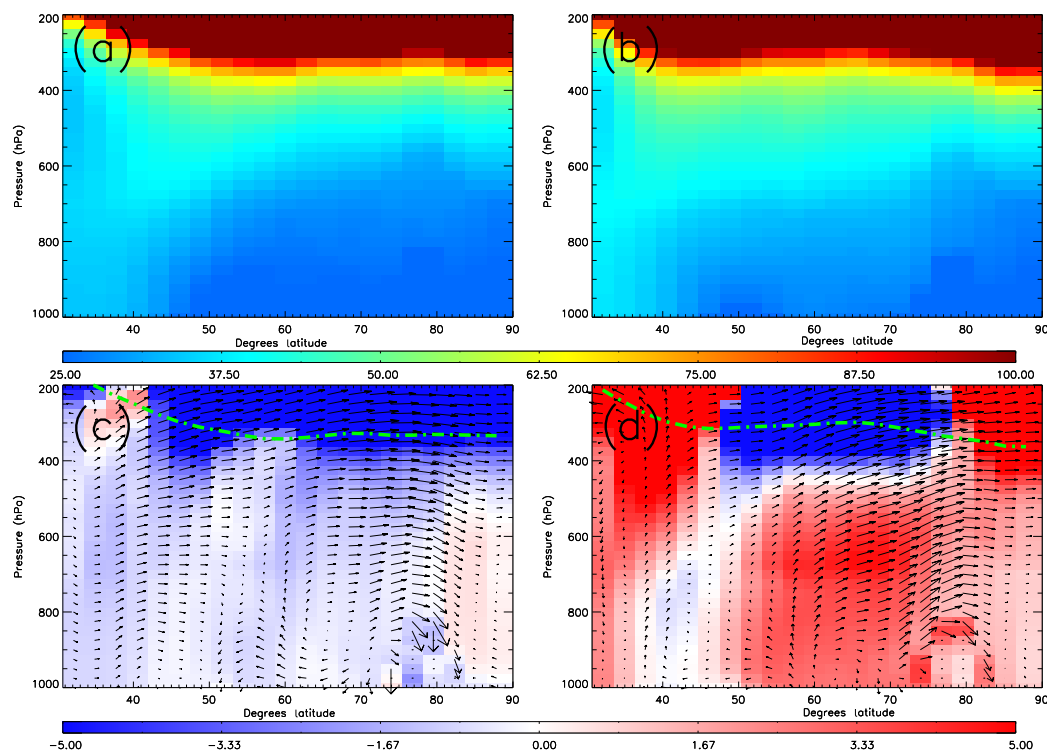


Figure 15. TOMCAT ozone (ppbv) cross section at 56.25° W averaged between 2006 and 2015 sampled under the wintertime (NDJF) NAO. Panel (a) NAO positive phase, (b) NAO negative phase, (c) shows the NAO positive phase anomaly relative to the wintertime average and (d) shows the negative NAO phase anomaly relative to the wintertime average. Green dashed lines represents the dynamical tropopause. Wind vectors represent the cross section (56.25° W) meridional and vertical (scaled by 10^4) winds.

of the NAO circulation in the upper troposphere, where NO_2 concentrations are much lower. Under NAO-low, the reduced westerly flow significantly aids the accumulation of NO_2 at levels between the surface and approximately 600 hPa. This is important for air pollution levels over source regions which are predominately highly polluted and populated. Ozone has the opposite signal to NO_2 in the lower troposphere where NAO-high replaces primary polluted air (e.g. high NO_x content) over Europe with ozone-enriched Atlantic air masses. The high ozone content of these air masses is linked to ozone formed downwind of primary pollution from North America and decreased levels of ozone-depleting gases (e.g. NO , when photochemical and OH activity are slower) over Europe. Over North America and the western North Atlantic, NAO-high and NAO-low show significant decreases and increases in tropospheric ozone, respectively, as the NAO-high enhanced westerlies transport ozone-enriched air masses towards Europe, while NAO-low weakens this transport pathway, resulting in elevated ozone concentration in the region from North American pollution outflow.

In the UTLS, the spatial distribution of PAN is heavily influenced by both horizontal and vertical transport. In NAO-high, as shown by MIPAS (see Supplement) and Fig. 11, the tropopause height is elevated, enhancing the vertical trans-

port of PAN into the UTLS over the Arctic and subtropical North Atlantic. UTLS horizontal winds also contribute to these elevated PAN concentrations as strong winds (e.g. 30 m s^{-1}) help accumulate PAN in the Arctic. In NAO-low, poleward flow from the subtropical North Atlantic has weakened, leading to a decrease in PAN over the North Atlantic and there is no longer the accumulation of Arctic PAN. However, the UTLS anticyclone (as seen in Fig. 1e) shows a clear accumulation of PAN in the UTLS over southern Greenland and Iceland linked to vertical transport of PAN from the pollutant lower troposphere over Europe (reduced westerlies in NAO-low allow the accumulation of PAN and NO_x). Ozone in the troposphere and UTLS is anti-correlated with PAN, which we show to be transport dominated, highlighting regions of air mass intrusions from the troposphere into the stratosphere and vice versa. For instance, in the UTLS Iceland–southern Greenland anticyclone ozone is significantly reduced while PAN is enhanced. In winter, as photochemical activity and reaction with OH are reduced, polluted air masses with high NO_x content will yield low ozone and high PAN concentrations, respectively. However, stratospheric intrusions into the upper troposphere (e.g. Fig. 14d between 40 and 60° N) have a high ozone content but low

PAN concentrations as there is limited production of PAN in this part of the atmosphere.

5 Conclusions

This study has used state-of-the-art satellite data records of atmospheric trace gases to identify recent influences of the North Atlantic Oscillation (NAO) on tropospheric composition over the North Atlantic and Europe. We have used tropospheric column NO₂ (TCNO₂) measurements from the Ozone Monitoring Instrument (OMI), which provides higher resolution and sampling than past instruments to detect clear and significant responses (i.e. reduction in UK TCNO₂ during NAO-high) from NAO circulation patterns, building on the initial signal reported by Eckhardt et al. (2003). Vertical profiles of ozone from the Tropospheric Emissions Spectrometer (TES) allow a detailed assessment of satellite-observed lower-tropospheric ozone sampled under the NAO phases. Robust, statistically significant signals are found on both sides of the North Atlantic as a result of changes in the westerly circulation during the two NAO phases. Finally, peroxyacetyl nitrate (PAN) observations in the upper troposphere–lower stratosphere (UTLS) from the Michelson Interferometer for Passive Atmospheric Sounding (MIPAS) are exploited, given the long lifetime of PAN (several months, Singh et al., 1996), for the first time to investigate vertical transport of polluted tropospheric air masses into the UTLS under different NAO conditions.

Our results, supported by simulations from the TOMCAT chemistry transport model (CTM), confirm that primary pollutant (i.e. NO₂) concentrations are reduced (enhanced) under NAO-high (NAO-low) conditions over Europe and are heavily dependent on the strength of the westerly flow across the Atlantic. However, secondary pollutants, such as ozone, have anti-correlated patterns as maritime air masses (ozone-enriched air formed downwind from North American primary pollutant emissions) disperse polluted European air masses under NAO-high conditions, significantly increasing the background ozone levels. Under NAO-low conditions, the slackening of the North Atlantic westerly flow allows for the accumulation of primary pollutants over Europe, where ozone concentrations are further decreased by ozone titration (loss through reaction with nitric oxide, NO). Different responses to those over Europe are observed and simulated by TES and TOMCAT over the western North Atlantic where enhanced westerly flow (NAO-high conditions) yields lower ozone concentrations over eastern North America through pollutant (both ozone and ozone precursors) long-range transport towards Europe. However, the weakening of the westerly flow (NAO-low conditions) allows ozone to accumulate and form over the region. We also find that NAO circulation is important for UTLS composition as polluted air masses (e.g. with high PAN content) originating from Europe during NAO-low (accumulation of lower-

tropospheric pollution) can propagate to this altitude, resulting in elevated PAN concentrations over Iceland and southern Greenland. Model simulations show that UTLS ozone spatial patterns over the North Atlantic are strongly anti-correlated to those of PAN, whereby the two trace gases act as flags for polluted tropospheric and clean stratospheric air in the UTLS.

Overall, the use of recent satellite data sets, not used in context of the NAO before, and a model simulation have quantified the recent influences of the NAO on tropospheric composition and co-variability between pollutants.

Data availability. The OMI tropospheric column NO₂ data (DOMINO product v2.0) come from the Tropospheric Emission Monitoring Internet Service (TEMIS), which is available at <http://www.temis.nl/airpollution/no2.html> (Tropospheric Emissions Monitoring Internet Service, 2017). The surface data from AURN can be found at <https://uk-air.defra.gov.uk/networks/network-info?view=aurndata> (Department for Environment, Food and Rural Affairs, 2017). Lerwick ozonesonde data provided by the World Ozone and Ultraviolet Radiation Data Centre are from <http://woudc.org/> (World Ozone and Ultraviolet Radiation Data Centre, 2017). North Atlantic Oscillation Index data, from the Climatic Research Unit, University of East Anglia, is from <https://crudata.uea.ac.uk/cru/data/nao> (Climate Research Unit – University of East Anglia, 2017). TES ozone data are provided by NASA's JPL <https://search.earthdata.nasa.gov/> (Jet Propulsion Laboratory – NASA, 2017) and MIPAS data are from KIT (<https://www.imk-asf.kit.edu/english/308.php>, Karlsruhe Institute of Technology, 2017). The model simulations from TOMCAT can be found at http://homepages.see.leeds.ac.uk/~earrjpo/acp_data_nao/ (Pope et al., 2018b).

The Supplement related to this article is available online at <https://doi.org/10.5194/acp-18-8389-2018-supplement>.

Competing interests. The authors declare that they have no conflict of interest.

Acknowledgements. This work was supported by the NERC National Centre for Earth Observation (NCEO). TOMCAT modelling development was supported by the National Centre for Atmospheric Science (NCAS). Simulations were performed on the national Archer and Leeds ARC HPC systems. We acknowledge the use of the Tropospheric Emission Monitoring Internet Service (TEMIS) OMI tropospheric column NO₂ data (DOMINO product v2.0). We also acknowledge the use of data from AURN supported by the Department of Environment, Food and Rural Affairs (DEFRA) and Lerwick ozonesonde data provided by the World Ozone and Ultraviolet Radiation Data Centre. We also thank the Climatic Research Unit, University of East Anglia for the use of their North Atlantic Oscillation Index data. Finally, we acknowledge the use of the TES ozone data provided by NASA's JPL and MIPAS data

from KIT.

Edited by: Andrea Pozzer

Reviewed by: three anonymous referees

References

- Bacer, S., Christoudias, T., and Pozzer, A.: Projection of North Atlantic Oscillation and its effect on tracer transport, *Atmos. Chem. Phys.*, 16, 15581–15592, <https://doi.org/10.5194/acp-16-15581-2016>, 2016.
- Boersma, K., Braak, R., and van der A, R.: Dutch OMI NO₂ (DOMINO) data product v2.0, Tropospheric Emissions Monitoring Internet Service on-line documentation, p. available at: http://www.temis.nl/docs/OMI_NO2_HE5_2.0_2011.pdf (last access: June 2017), 2011.
- Boersma, K. F., Eskes, H. J., and Brinksma, E. J.: Error analysis for tropospheric NO₂ retrieval from space, *J. Geophys. Res.-Atmos.*, 109, d04311, <https://doi.org/10.1029/2003JD003962>, 2004.
- Boersma, K. F., Eskes, H. J., Veeffkind, J. P., Brinksma, E. J., van der A, R. J., Sneep, M., van den Oord, G. H. J., Levelt, P. F., Stammes, P., Gleason, J. F., and Bucsela, E. J.: Near-real time retrieval of tropospheric NO₂ from OMI, *Atmos. Chem. Phys.*, 7, 2103–2118, <https://doi.org/10.5194/acp-7-2103-2007>, 2007.
- Braak, R.: Row Anomaly Flagging Rules Lookup Table, KNMI Technical Document TN-OMIE-KNMI-950, 2010.
- Chipperfield, M. P.: New version of the TOMCAT/SLIMCAT off-line chemical transport model: Intercomparison of stratospheric tracer experiments, *Q. J. Roy. Meteor. Soc.*, 132, 1179–1203, <https://doi.org/10.1256/qj.05.51>, 2006.
- Christoudias, T., Pozzer, A., and Lelieveld, J.: Influence of the North Atlantic Oscillation on air pollution transport, *Atmos. Chem. Phys.*, 12, 869–877, <https://doi.org/10.5194/acp-12-869-2012>, 2012.
- Cohen, R. C., Wennberg, P. O., Stimpfle, R. M., Koplów, J., Anderson, J. G., Fahey, D. W., Woodbridge, E. L., Keim, E. R., Gao, R., Proffitt, M. H., Loewenstein, M., and Chan, K. R.: Are models of catalytic removal of O₃ by HO_x accurate? Constraints from in situ measurements of the OH to HO₂ ratio, *Geophysical Research Letters*, 21, 2539–2542, <https://doi.org/10.1029/94GL01713>, 1994.
- Creilson, J. K., Fishman, J., and Wozniak, A. E.: Intercontinental transport of tropospheric ozone: a study of its seasonal variability across the North Atlantic utilizing tropospheric ozone residuals and its relationship to the North Atlantic Oscillation, *Atmos. Chem. Phys.*, 3, 2053–2066, <https://doi.org/10.5194/acp-3-2053-2003>, 2003.
- Dee, D. P., Uppala, S. M., Simmons, A. J., Berrisford, P., Poli, P., Kobayashi, S., Andrae, U., Balmaseda, M. A., Balsamo, G., Bauer, P., Bechtold, P., Beljaars, A. C. M., van de Berg, L., Bidlot, J., Bormann, N., Delsol, C., Dragani, R., Fuentes, M., Geer, A. J., Haimberger, L., Healy, S. B., Hersbach, H., Hólm, E. V., Isaksen, I., Kållberg, P., Köhler, M., Matricardi, M., McNally, A. P., Monge-Sanz, B. M., Morcrette, J.-J., Park, B.-K., Peubey, C., de Rosnay, P., Tavolato, C., Thépaut, J.-N., and Vitart, F.: The ERA-Interim reanalysis: configuration and performance of the data assimilation system, *Q. J. Roy. Meteor. Soc.*, 137, 553–597, <https://doi.org/10.1002/qj.828>, 2011.
- DEFRA: Automated Urban and Rural Network (AURN), available at: uk-air.defra.gov.uk/networks/network-info?view=aur (last access: June 2017), 2015.
- Department for Environment, Food and Rural Affairs: Automatic Urban and Rural Network (AURN), available at: <https://uk-air.defra.gov.uk/networks/network-info?view=aur>, last access: June 2017.
- Eckhardt, S., Stohl, A., Beirle, S., Spichtinger, N., James, P., Forster, C., Junker, C., Wagner, T., Platt, U., and Jennings, S. G.: The North Atlantic Oscillation controls air pollution transport to the Arctic, *Atmos. Chem. Phys.*, 3, 1769–1778, <https://doi.org/10.5194/acp-3-1769-2003>, 2003.
- Edwards, D. P., Emmons, L. K., Hauglustaine, D. A., Chu, D. A., Gille, J. C., Kaufman, Y. J., Pétron, G., Yurganov, L. N., Giglio, L., Deeter, M. N., Yudin, V., Ziskin, D. C., Warner, J., Lamarque, J.-F., Francis, G. L., Ho, S. P., Mao, D., Chen, J., Grechko, E. I., and Drummond, J. R.: Observations of carbon monoxide and aerosols from the Terra satellite: Northern Hemisphere variability, *J. Geophys. Res.-Atmos.*, 109, d24202, <https://doi.org/10.1029/2004JD004727>, 2004.
- Emmons, L. K., Arnold, S. R., Monks, S. A., Huijnen, V., Tilmes, S., Law, K. S., Thomas, J. L., Raut, J.-C., Bouarar, I., Turquety, S., Long, Y., Duncan, B., Steenrod, S., Strode, S., Flemming, J., Mao, J., Langner, J., Thompson, A. M., Tarasick, D., Apel, E. C., Blake, D. R., Cohen, R. C., Dibb, J., Diskin, G. S., Fried, A., Hall, S. R., Huey, L. G., Weinheimer, A. J., Wisthaler, A., Mikoviny, T., Nowak, J., Weischl, J., Roberts, J. M., Ryerson, T., Warneke, C., and Helmig, D.: The POLARCAT Model Intercomparison Project (POLMIP): overview and evaluation with observations, *Atmos. Chem. Phys.*, 15, 6721–6744, <https://doi.org/10.5194/acp-15-6721-2015>, 2015.
- Eskes, H. J. and Boersma, K. F.: Averaging kernels for DOAS total-column satellite retrievals, *Atmos. Chem. Phys.*, 3, 1285–1291, <https://doi.org/10.5194/acp-3-1285-2003>, 2003.
- Fischer, H., Birk, M., Blom, C., Carli, B., Carlotti, M., von Clarmann, T., Delbouille, L., Dudhia, A., Ehrt, D., Endemann, M., Flaud, J. M., Gessner, R., Kleinert, A., Koopman, R., Langen, J., López-Puertas, M., Mosner, P., Nett, H., Oelhaf, H., Perron, G., Remedios, J., Ridolfi, M., Stiller, G., and Zander, R.: MIPAS: an instrument for atmospheric and climate research, *Atmos. Chem. Phys.*, 8, 2151–2188, <https://doi.org/10.5194/acp-8-2151-2008>, 2008.
- Glatthor, N., von Clarmann, T., Fischer, H., Funke, B., Grabowski, U., Höpfner, M., Kellmann, S., Kiefer, M., Linden, A., Milz, M., Steck, T., and Stiller, G. P.: Global peroxyacetyl nitrate (PAN) retrieval in the upper troposphere from limb emission spectra of the Michelson Interferometer for Passive Atmospheric Sounding (MIPAS), *Atmos. Chem. Phys.*, 7, 2775–2787, <https://doi.org/10.5194/acp-7-2775-2007>, 2007.
- Granier, C., Bessagnet, B., Bond, T., D'Angiola, A., Denier van der Gon, H., Frost, G. J., Heil, A., Kaiser, J. W., Kinne, S., Klimont, Z., Kloster, S., Lamarque, J.-F., Lioussé, C., Masui, T., Meuleux, F., Mieville, A., Ohara, T., Raut, J.-C., Riahi, K., Schultz, M. G., Smith, S. J., Thompson, A., Aardenne, J., Werf, G. R., and Vuuren, D. P.: Evolution of anthropogenic and biomass burning emissions of air pollutants at global and regional scales during the 1980–2010 period, *Clim. Chang.*, 109, 163–190, <https://doi.org/10.1007/s10584-011-0154-1>, 2011.

- Hurrell, J. W.: Decadal Trends in the North Atlantic Oscillation: Regional Temperatures and Precipitation, *Science*, 269, 676–679, <https://doi.org/10.1126/science.269.5224.676>, 1995.
- Hurrell, J. W. and Deser, C.: North Atlantic climate variability: The role of the North Atlantic Oscillation, Impact of climate variability on marine ecosystems: A comparative approach, *J. Marine Syst.*, 79, 231–244, <https://doi.org/10.1016/j.jmarsys.2009.11.002>, 2010.
- Jet Propulsion Laboratory – NASA: Earth Data Search, available at: <https://search.earthdata.nasa.gov/search>, last access: June 2017.
- Jones, P. D., Jonsson, T., and Wheeler, D.: Extension to the North Atlantic oscillation using early instrumental pressure observations from Gibraltar and south-west Iceland, *Int. J. Climatol.*, 17, 1433–1450, [https://doi.org/10.1002/\(SICI\)1097-0088\(19971115\)17:13<1433::AID-JOC203>3.0.CO;2-P](https://doi.org/10.1002/(SICI)1097-0088(19971115)17:13<1433::AID-JOC203>3.0.CO;2-P), 1997.
- Karlsruhe Institute of Technology: MIPAS/ENVISAT data, available at: <https://www.imk-asf.kit.edu/english/308.php>, last access: June 2017.
- Mann, G. W., Carslaw, K. S., Spracklen, D. V., Ridley, D. A., Manktelow, P. T., Chipperfield, M. P., Pickering, S. J., and Johnson, C. E.: Description and evaluation of GLOMAP-mode: a modal global aerosol microphysics model for the UKCA composition-climate model, *Geosci. Model Dev.*, 3, 519–551, <https://doi.org/10.5194/gmd-3-519-2010>, 2010.
- McNorton, J., Chipperfield, M. P., Gloor, M., Wilson, C., Feng, W., Hayman, G. D., Rigby, M., Krummel, P. B., O'Doherty, S., Prinn, R. G., Weiss, R. F., Young, D., Dlugokencky, E., and Montzka, S. A.: Role of OH variability in the stalling of the global atmospheric CH₄ growth rate from 1999 to 2006, *Atmos. Chem. Phys.*, 16, 7943–7956, <https://doi.org/10.5194/acp-16-7943-2016>, 2016.
- Monks, S. A., Arnold, S. R., Hollaway, M. J., Pope, R. J., Wilson, C., Feng, W., Emmerson, K. M., Kerridge, B. J., Latter, B. L., Miles, G. M., Siddans, R., and Chipperfield, M. P.: The TOMCAT global chemical transport model v1.6: description of chemical mechanism and model evaluation, *Geosci. Model Dev.*, 10, 3025–3057, <https://doi.org/10.5194/gmd-10-3025-2017>, 2017.
- Osborn, T. J.: Recent variations in the winter North Atlantic Oscillation, *Weather*, 61, 353–355, <https://doi.org/10.1256/wea.190.06.2006>.
- Pausata, F. S. R., Pozzoli, L., Vignati, E., and Dentener, F. J.: North Atlantic Oscillation and tropospheric ozone variability in Europe: model analysis and measurements intercomparison, *Atmos. Chem. Phys.*, 12, 6357–6376, <https://doi.org/10.5194/acp-12-6357-2012>, 2012.
- Pirovano, G., Balzarini, A., Bessagnet, B., Emery, C., Kallos, G., Meleux, F., Mitsakou, C., Nopmongcol, U., Riva, G., and Yarwood, G.: Investigating impacts of chemistry and transport model formulation on model performance at European scale, aQMEII: An International Initiative for the Evaluation of Regional-Scale Air Quality Models – Phase 1, *Atmos. Environ.*, 53, 93–109, <https://doi.org/10.1016/j.atmosenv.2011.12.052>, 2012.
- Pope, R. J., Savage, N. H., Chipperfield, M. P., Arnold, S. R., and Osborn, T. J.: The influence of synoptic weather regimes on UK air quality: analysis of satellite column NO₂, *Atmos. Sci. Lett.*, 15, 211–217, <https://doi.org/10.1002/asl2.492>, 2014.
- Pope, R. J., Chipperfield, M. P., Savage, N. H., Ordóñez, C., Neal, L. S., Lee, L. A., Dhomse, S. S., Richards, N. A. D., and Keslake, T. D.: Evaluation of a regional air quality model using satellite column NO₂: treatment of observation errors and model boundary conditions and emissions, *Atmos. Chem. Phys.*, 15, 5611–5626, <https://doi.org/10.5194/acp-15-5611-2015>, 2015.
- Pope, R. J., Richards, N. A. D., Chipperfield, M. P., Moore, D. P., Monks, S. A., Arnold, S. R., Glatthor, N., Kiefer, M., Breider, T. J., Harrison, J. J., Remedios, J. J., Warneke, C., Roberts, J. M., Diskin, G. S., Huey, L. G., Wisthaler, A., Apel, E. C., Bernath, P. F., and Feng, W.: Intercomparison and evaluation of satellite peroxyacetyl nitrate observations in the upper troposphere-lower stratosphere, *Atmos. Chem. Phys.*, 16, 13541–13559, <https://doi.org/10.5194/acp-16-13541-2016>, 2016.
- Pope, R. J., Arnold, S. R., Chipperfield, M. P., Latter, B. G., Siddans, R., and Kerridge, B. J.: Widespread changes in UK air quality observed from space, *Atmos. Sci. Lett.*, 1–8, <https://doi.org/10.1002/asl.817>, 2018a.
- Pope, R. J., Feng, W., and Chipperfield, M. P.: Index of /~earrjpo/acp_data_ao/, available at: http://homepages.se.leeds.ac.uk/~earrjpo/acp_data_ao/, last access: June 2018b.
- Quinn, P. K., Shaw, G., Andrews, E., Dutton, E. G., Ruoho-Airola, T., and Gong, S. L.: Arctic haze: current trends and knowledge gaps, *Tellus B*, 59, 99–114, <https://doi.org/10.1111/j.1600-0889.2006.00238.x>, 2007.
- Randerson, J. T., van der Werf, G. R., Giglio, L., Collatz, G. J., and Kasibhatla, P. S.: Global Fire Emissions Database, Version 3 (GFEDv3.1), Data set, available at: <http://daac.ornl.gov/> (last access: June 2015), from Oak Ridge National Laboratory Distributed Active Archive Center, Oak Ridge, Tennessee, USA, available at: https://daac.ornl.gov/cgi-bin/dsvviewer.pl?ds_id=1191 (last access: June 2015), 2013.
- Richards, N. A. D., Osterman, G. B., Browell, E. V., Hair, J. W., Avery, M., and Li, Q.: Validation of Tropospheric Emission Spectrometer ozone profiles with aircraft observations during the Intercontinental Chemical Transport Experiment–B, *J. Geophys. Res.-Atmos.*, 113, d16S29, <https://doi.org/10.1029/2007JD008815>, 2008.
- Richards, N. A. D., Arnold, S. R., Chipperfield, M. P., Miles, G., Rap, A., Siddans, R., Monks, S. A., and Hollaway, M. J.: The Mediterranean summertime ozone maximum: global emission sensitivities and radiative impacts, *Atmos. Chem. Phys.*, 13, 2331–2345, <https://doi.org/10.5194/acp-13-2331-2013>, 2013.
- Singh, H. B.: Reactive nitrogen in the troposphere, *Environ. Sci. Technol.*, 21, 320–327, <https://doi.org/10.1021/es00158a001>, 1987.
- Singh, H. B., Herlth, D., Kolyer, R., Chatfield, R., Viezee, W., Salas, L. J., Chen, Y., Bradshaw, J. D., Sandholm, S. T., Talbot, R., Gregory, G. L., Anderson, B., Sachse, G. W., Browell, E., Bachmeier, A. S., Blake, D. R., Heikes, B., Jacob, D., and Fuelberg, H. E.: Impact of biomass burning emissions on the composition of the South Atlantic troposphere: Reactive nitrogen and ozone, *J. Geophys. Res.-Atmos.*, 101, 24203–24219, <https://doi.org/10.1029/96JD01018>, 1996.
- Stohl, A.: Characteristics of atmospheric transport into the Arctic troposphere, *J. Geophys. Res.-Atmos.*, 111, d11306, <https://doi.org/10.1029/2005JD006888>, 2006.
- Thomas, M. A. and Devasthale, A.: Sensitivity of free tropospheric carbon monoxide to atmospheric weather states and their persistency: an observational assessment over the

- Nordic countries, *Atmos. Chem. Phys.*, 14, 11545–11555, <https://doi.org/10.5194/acp-14-11545-2014>, 2014
- Trigo, I. F.: Climatology and interannual variability of stormtracks in the Euro-Atlantic sector: a comparison between ERA-40 and NCEP/NCAR reanalyses, *Clim. Dynam.*, 26, 127–143, <https://doi.org/10.1007/s00382-005-0065-9>, 2006.
- Tropospheric Emissions Monitoring Internet Service: Tropospheric Column NO₂ from satellite, available at: <http://www.temis.nl/airpollution/no2.html>, last access: June 2017.
- Wiegele, A., Glatthor, N., Höpfner, M., Grabowski, U., Kellmann, S., Linden, A., Stiller, G., and von Clarmann, T.: Global distributions of C₂H₆, C₂H₂, HCN, and PAN retrieved from MIPAS reduced spectral resolution measurements, *Atmos. Meas. Tech.*, 5, 723–734, <https://doi.org/10.5194/amt-5-723-2012>, 2012.
- Worden, H. M., Edwards, D. P., Deeter, M. N., Fu, D., Kulawik, S. S., Worden, J. R., and Arellano, A.: Averaging kernel prediction from atmospheric and surface state parameters based on multiple regression for nadir-viewing satellite measurements of carbon monoxide and ozone, *Atmos. Meas. Tech.*, 6, 1633–1646, <https://doi.org/10.5194/amt-6-1633-2013>, 2013.
- World Ozone and Ultraviolet Radiation Data Centre: WOUDC-Home, available at: <http://woudc.org>, last access June 2017.
- Zhou, Y., Brunner, D., Hueglin, C., Henne, S., and Staehelin, J.: Changes in {OMI} tropospheric {NO₂} columns over Europe from 2004 to 2009 and the influence of meteorological variability, *Atmos. Environ.*, 46, 482–495, <https://doi.org/10.1016/j.atmosenv.2011.09.024>, 2012.